NASA TECHNICAL MEMORANDUM

NASA TM X-3212

NASA TM X-3212

ABORT SEPARATION STUDY OF A SHUTTLE ORBITER AND EXTERNAL TANK AT HYPERSONIC SPEEDS

Peter T. Bernot

Langley Research Center
Hampton, Va. 23665

NATIONAL AERONAUTICS AND SPACE ADMINISTRATION • WASHINGTON, D. C. • MAY 1975

1. Report No.	2. Government Accession No.	3. Recipient's Catalog No.
NASA TM X-3212		

4. Title and Subtitle	5. Report Date
ABORT SEPARATION STUDY OF A SHUTTLE ORBITER AND EXTERNAL TANK AT HYPERSONIC SPEEDS	May 1975
	6. Performing Organization Code
7. Author(s)	8. Performing Organization Report No.
Peter T. Bernot	L-10073
	10. Work Unit No.
9. Performing Organization Name and Address	506-26-10-06
NASA Langley Research Center Hampton, Va. 23665	11. Contract or Grant No.
	13. Type of Report and Period Covered
12. Sponsoring Agency Name and Address	Technical Note
National Aeronautics and Space Administration Washington, D.C. 20546	14. Sponsoring Agency Code

15. Supplementary Notes

16. Abstract

An investigation has been performed to determine the effects of several parameters on the relative motions of an early Langley Research Center space shuttle orbiter design and its external tank during staging for the return-to-launch-site (RTLS) abort mode. The parameters included angle of attack, dynamic pressure, flight-path angle, pitch rate, elevon effectiveness, and the use of thrust applied to the tank. The relative positions of each component were determined by a separation trajectory computer program which incorporated data obtained in wind-tunnel tests with the orbiter and tank in proximity. These tests were conducted at Mach 10.3 in the Langley continuous-flow hypersonic tunnel. All separation cases were initiated at a constant Mach number of 10 with an assumed sideslip angle of 0°.

17. Key Words (Suggested by Author(s))	18. Distribution Statement
Space shuttle orbiter Abort separation Stability and control	Unclassified – Unlimited New Subject Category 16

19. Security Classif. (of this report)	20. Security Classif. (of this page)	21. No. of Pages	22. Price*
Unclassified	Unclassified	47	$3.75

*For sale by the National Technical Information Service, Springfield, Virginia 22151

ABORT SEPARATION STUDY OF A SHUTTLE ORBITER AND EXTERNAL TANK AT HYPERSONIC SPEEDS

Peter T. Bernot
Langley Research Center

SUMMARY

The effects of several parameters on the relative motions of an early Langley Research Center space shuttle orbiter design and its external tank have been determined at Mach 10 during staging for the return-to-launch-site abort mode. The parameters studied included angle of attack, dynamic pressure, flight-path angle, pitch rate, elevon effectiveness, and the use of thrust applied to the tank. The relative positions of each vehicle during staging were determined by a separation computer program which incorporated data obtained in wind-tunnel tests with the orbiter and tank in proximity. These tests were conducted at Mach 10.3 in the Langley continuous-flow hypersonic tunnel.

The results of this study indicated that successful separation was possible by initiating release at angles of attack between -4° and -10°. As dynamic pressure increased, separation distance increased for an initial angle of attack of -4° because of favorable effects on the pitch rates of both components. Variation of flight-path angle had minor effects on the vehicle motions. Minimal benefits were obtained by variation of initial pitch rate.

An assumed rocket thrust vector applied to the tank resulted in safe separations at angles of attack up to 30°. Plume effects on the aerodynamic characteristics of the components were, however, not taken into account. Thrust magnitudes required for safe separation were reduced by a factor of about 2 by alining the thrust vector normal to the tank center line compared with the thrust vector acting through the tank center of gravity at an inclination angle of 38° to the center line.

INTRODUCTION

For the return-to-launch-site (RTLS) abort mode, the space shuttle orbiter must separate safely from its external tank in the sensible atmosphere. Trajectory studies have indicated that the staging occurs at low hypersonic speeds (Mach numbers from 6 to 7) and at relatively low values of dynamic pressure. Analyses of the relative motions of both components during staging have been made by using component aerodynamic characteristics measured in proximity in a separation analysis computer program which inte-

grates the equations of motion. By performing the analyses at various flight conditions, boundaries can be defined where recontact (collision) between the components will not occur.

The purpose of this report is to show the effects of several parameters on the staging motions at Mach 10 of an orbiter and its external tank which were designed at Langley Research Center. The full-scale orbiter, designed for reduced length and payload bay access at the aft end of the fuselage, incorporated a payload bay that was 18.3 m (60 ft) long with a diameter of 4.6 m (15 ft). Previous wind-tunnel results for this orbiter configuration were reported in reference 1. The parameters investigated in the present report include angle of attack, dynamic pressure, pitch rate, flight-path angle, and elevon effectiveness. The application of separation thrust to the external tank was also examined.

Longitudinal aerodynamic characteristics of the orbiter and tank in proximity were experimentally obtained at Mach 10.3 in the Langley continuous-flow hypersonic tunnel. A dual force balance system was used to measure the forces and moments simultaneously on each model at various axial and vertical spacings for relative incidence angles from -5° to 10°. A few tests were also made with the orbiter elevons deflected to assess tank interference on elevon effectiveness. These experimental results were incorporated in a computer program (ref. 2) which solves the equations of motion of each component and determines their relative positions and attitude during a staging maneuver. For each separation case, pictorial representations of the orbiter and tank showing their relative positions throughout the staging maneuver were generated by the computer and are used extensively in this report.

SYMBOLS

The aerodynamic loads for each model have been reduced into coefficient form with respect to its own body-axis system. The location of the origin and the orientation of the body axes are shown in figures 1 and 2. The geometric constants used to reduce the aerodynamic loads into coefficient form are indicated in table I. Although values are given in both SI Units and U.S. Customary Units in this report, the measurements and calculations for the investigation were made in U.S. Customary Units.

C_A axial-force coefficient, $\frac{\text{Axial force}}{q_\infty S}$

C_m pitching-moment coefficient, $\frac{\text{Pitching moment}}{q_\infty Sc}$

C_N normal-force coefficient, $\frac{\text{Normal force}}{q_\infty S}$

c	reference length (see table I); mean aerodynamic chord for orbiter and body length for tank, cm (in.)
d	tank diameter, cm (in.)
I_Y	mass moment of inertia about pitch axis, kg-m^2 (slug-ft^2)
q_∞	free-stream dynamic pressure, N/m^2 (lb/ft^2)
S	reference area (see table I), total wing planform for orbiter and maximum cross section for tank, cm^2 (in^2)
t	time, sec
x,z	axial and vertical spacing variables of tank moment reference point relative to orbiter moment reference point (see fig. 4), cm (in.)
α	angle of attack, deg
α_i	incidence angle between orbiter and tank, $\alpha_o - \alpha_t$, deg
γ	initial flight-path angle, deg
δ_e	elevon deflection angle, positive with trailing edge down, deg
ϵ	inclination of assumed rocket thrust vector relative to tank center line (see fig. 5), deg
$\dot{\theta}$	pitch rate, deg/sec

Subscripts:

o	orbiter
t	tank

MODELS AND APPARATUS

The orbiter model was a 0.0075-scale version of an early orbiter concept (fig. 1) designed at Langley Research Center for reduced length and payload bay access at the aft end of the fuselage. The cast aluminum model had a clipped delta wing, vertical tail, and body flap. The model of the external tank (fig. 2), designed to carry liquid-oxygen and liquid-hydrogen propellants, was machined from aluminum. External hardware attachments such as struts and propellant lines were not simulated on the models. Geometric characteristics of both models are presented in table I.

Experimental aerodynamic data were obtained in the Langley continuous-flow hypersonic tunnel which has a 0.79-m (31-in.) square test section. This facility is a closed-circuit type with five compressors for circulating the air flow. Electrical resistance tube bundles heat the air to sufficiently high temperatures to prevent liquefaction. This facility was designed to operate at pressures of 15 to 150 atm (1 atm = 0.101 MN/m^2) and at temperatures up to 1083 K (1950° R). Additional details are presented in reference 3.

Forces and moments were measured by water-cooled, six-component, strain-gage balances attached to a remotely controlled strut mechanism. For the orbiter-alone tests, a single balance-sting assembly was attached to the strut which was located on the tunnel center line. For the orbiter-tank proximity tests, a second balance-sting assembly was supported relative to the first by a streamlined plate which was bolted to the orbiter sting. Figure 3 is a photograph of this setup. This entire assembly was mounted on a hydraulically actuated injection mechanism which permitted insertion into the airstream from a sealed cooling chamber attached to the test section.

TESTS AND DATA REDUCTION

The wind-tunnel tests were conducted at a stagnation pressure of 5.17 MN/m^2 (750 psia) and a temperature of 1011 K (1820° R). The free-stream Mach number was 10.3 and the free-stream Reynolds number was 3.3×10^6 per meter (1.0×10^6 per foot). For the proximity tests, simultaneous data were obtained on both models over an angle-of-attack range from -10° to 35° at each of the 12 axial-vertical spacings indicated in figure 4. The spacing variables x and z were based on the positions of the tank moment reference point relative to the orbiter moment reference point. Data were also obtained at incidence angles from -5° to 10° as presented in table II. The desired spacing and incidence angle α_i were preset by manually displacing the tank-sting assembly. Angles of attack have been corrected for deflection of sting and balance due to aerodynamic loads. Most tests were made with the elevons and body flap undeflected; however, a few tests were performed with elevon deflections of -20° and -40°.

METHOD OF ANALYSIS

An expanded version of the computer program of reference 2 was used to determine the relative motions of each vehicle during the staging maneuver. Assuming zero sideslip, the equations of motion for each vehicle were restricted to three degrees of freedom. The experimentally measured values of C_N, C_A, and C_m were arranged into a matrix as functions of the spacing variables x and z, incidence angle, and vehicle angle of attack. The computer program numerically integrated the equations of motion in stepwise fashion. The values of the aerodynamic coefficients were obtained by linear interpolation between the discrete points of the wind-tunnel aerodynamic matrix at each integration step. Damping and rotary derivatives were assumed to be zero because of the high flight speed and relatively low dynamic pressure. For most computer runs, the iteration procedure did not exceed 8 sec, since collision or safe separation usually occurred within this time span.

Effects of angle of attack, dynamic pressure, flight-path angle, pitch rate, elevon deflection, and the use of a separation rocket on the tank were investigated. Incremental values of C_N and C_m due to negative elevon deflection were incorporated into the trajectory program. The selected elevon deflection angle remained fixed during each separation case. For those cases involving the assumed separation rocket on the tank, the thrust remained constant throughout the separation maneuver. However, the effects of the rocket plume on the aerodynamic characteristics of the orbiter and tank have not been taken into account. As shown in figure 5, the thrust vectors were applied at the tank interstage location and were directed either normal to the tank center line ($\epsilon = 90^o$) or through the tank center of gravity ($\epsilon = 38^o$). Vehicle characteristics used in this analysis are presented in the following table:

Component	Mass		I_Y	
	kg	lb	kg-m^2	slug-ft^2
Orbiter	79 868	176 080	6 928 000	5 110 000
Tank	30 243	66 674	4 786 000	3 530 000

The analysis was performed at a Mach number of 10 at three selected values of dynamic pressure. The staging conditions are summarized in the following table:

Dynamic pressure		Velocity		Altitude	
N/m^2	psf	m/sec	fps	km	ft
239.4	5	2889.5	9 480	72.2	237 000
958.0	20	3096.8	10 160	63.4	208 000
2873.0	60	3267.5	10 720	54.9	180 000

RESULTS AND DISCUSSION

Experimental Results

The static longitudinal characteristics of the orbiter and tank in proximity are presented in figures 6 to 9. For reference, the interference-free (isolated) data are also shown in the figures. The experimental results indicate large interference effects on the static stability, normal-force, and axial-force characteristics of both the orbiter and the tank. The data are dependent on both vertical and axial spacing and on the incidence angle between the two components.

The orbiter longitudinal data for various elevon deflections are presented in figure 10 for both minimum and maximum vertical spacings. Incremental values of C_m were calculated from these data and are presented in figure 11. Comparison of the interference values with those obtained for the isolated orbiter shows that tank interference does not significantly affect elevon effectiveness below an angle of attack of 15^o. Incremental values of C_N, also calculated from the data of figure 10, showed a similar result but are not presented herein. It may be inferred from these results that analytical separation studies in the lower angle-of-attack range can include elevon-effectiveness parameters obtained from hypersonic tests on an isolated orbiter.

Separation Results

The computer-generated pictorial results afford a rapid evaluation of each separation case and are therefore used extensively in this report. For all cases, release started at $t = 0$ sec with the models in the mated position $(x/d = 0, \quad z/d = 0, \text{ and } \alpha_i = 0^o)$ as shown in figure 4.

The effects of initial angle of attack ($t = 0$ sec) at a dynamic pressure of 958 N/m^2 (20 psf) at $\delta_e = 0^o$ were determined at angles of attack from -10^o to 30^o. These results at $\alpha_o = \alpha_t = 10^o, 0^o$, and -4^o are presented in figure 12. The inherent instability of the tank required that the initial angle of attack be lowered to at least -4^o for safe separation. The data of figure 13, in which the effects of dynamic pressure at $\alpha_o = \alpha_t = -4^o$ are presented, show that the separation distance between the two vehicles increased as dynamic pressure increased because of favorable effects on the pitch rates of both components. Effects of flight-path angle are presented in figure 14 for $\alpha_o = \alpha_t = -4^o$. Varying the flight-path angle from 0^o to -20^o had only minor effects on the separation maneuver. This result is not surprising because of the relatively short flight time and small range of flight-path angle.

The effects of initial pitch rate for both components at a dynamic pressure of 2873 N/m^2 (60 psf) are presented in figure 15 for $\alpha_o = \alpha_t = -3^o, -4^o$, and -8^o. In

general, positive pitch rates resulted in the tank rotating nose down and contacting the aft end of the orbiter. Safe separation occurred at $\alpha_o = \alpha_t = -4^o$ and -8^o for zero pitch rate. Many additional separation cases were run (not presented pictorially) to establish a limiting angle-of-attack pitch-rate boundary for safe separation. This boundary, presented in figure 16, shows that variation of pitch rate offers minimal benefits, since the angle of attack for safe separation is increased from -4^o to only -2^o.

The reliability of the calculated trajectories for both components is dependent on the amount of measured data stored in the input matrix. To investigate the effects of a reduced input matrix, the computer program was modified to restrict the aerodynamic input matrix to values measured at zero incidence angle. In figure 17, results are presented at a dynamic pressure of 2873 N/m^2 (60 psf). At $\alpha_o = \alpha_t = 0^o$, use of the reduced aerodynamic matrix had little effect on the resulting vehicle motions. At $\alpha_o = \alpha_t = -4^o$, however, the vehicle motions were affected when the input matrix was reduced and recontact occurred at $t = 8$ sec. These results indicate that obtaining experimental data at nonzero values of α_i is important.

Since unassisted separations were not possible at positive angles of attack, assumed rocket thrust was applied to the external tank at its interstage location to investigate possible safe separations up to an angle of attack of 30^o. The assumed vectors were limited to two angular orientations; one was normal to the tank center line ($\epsilon = 90^o$) and the other was directed through the tank center of gravity ($\epsilon = 38^o$). (See fig. 5.) The rocket plume effects on the aerodynamic characteristics of the orbiter and tank were not taken into account. Presented in figures 18 to 21 are the effects of the thrust at initial angles of attack from 0^o to 30^o for a dynamic pressure of 958 N/m^2 (20 psf). At $\alpha_o = \alpha_t = 0^o$ (fig. 18), a thrust of 11.1 kN (2500 lb) was required at $\epsilon = 90^o$ to prevent tank pitch-up that occurred for the zero thrust condition. At $\epsilon = 38^o$, a higher thrust of 22.2 kN (5000 lb) was required for safe separation. Tank pitch-up did occur for this thrust inclination angle (fig. 18(c)), but the thrust was sufficient to drive the tank far enough aft to prevent recontact. This type of separation, involving tank pitch-up, also occurred at $\alpha_o = \alpha_t = 10^o$, 20^o, and 30^o as shown in figures 19(b), 20(b), and 21(b). Large increases in thrust were necessary for safe separation as the angle of attack increased for both values of thrust inclination angle ϵ. At these higher attitudes, the maximum elevon deflection of -40^o was used, since the orbiter exhibited sizable pitch-down characteristics because of tank interference, as shown in figure 6.

Many trajectory cases were run over the angle-of-attack range at the three values of dynamic pressure to determine the boundaries for safe thrusting separation (fig. 22) at $\epsilon = 90^o$ and 38^o. A comparison of the thrusts shows that the thrust magnitudes for $\epsilon = 38^o$ are about twice those for $\epsilon = 90^o$. Note that the linear trends of the boundaries could be altered by the inclusion of plume effects on the orbiter.

Effects of elevon deflection at $\alpha_o = \alpha_t = 10^o$ are presented in figure 23 for a dynamic pressure of 2873 N/m^2 (60 psf). The thrust was 222.4 kN (50 000 lb) at $\epsilon = 38^o$. Varying the elevon deflection from 0^o to -40^o had only a small effect on the vehicle motions during the critical part of staging (t = 0 to t = 3 sec). With further increase in time, the orbiter angle of attack was increased significantly with increasing elevon deflection, as shown in figure 23(b).

SUMMARY OF RESULTS

The effects of several parameters on the staging maneuvers of an early Langley Research Center space shuttle orbiter design and its external tank have been determined for the return-to-launch-site abort mode. Force and moment data for both vehicles in proximity were obtained at Mach 10.3 and were incorporated into a separation trajectory computer program. The results are as follows:

1. Based solely on interference aerodynamics for the angle-of-attack range from -10^o to 30^o, successful separation was possible by initiating release at angles of attack between -4^o and -10^o.

2. At an initial angle of attack of -4^o, separation distance increased as dynamic pressure increased because of favorable effects on the pitch rates of both components. Variation of flight-path angle had minor effect on vehicle motions.

3. Minimal benefits were obtained by variation of initial pitch rate, since the angle of attack for safe separation was increased from -4^o to only -2^o.

4. The use of rocket thrust applied to the tank resulted in safe separation at angles of attack up to 30^o. The effects of the plumes on the aerodynamic characteristics of the components were not, however, taken into account.

5. Thrust magnitudes required for safe separation were reduced by a factor of approximately 2 by alining the thrust vector normal to the tank center line compared with the vector acting through the tank center of gravity at an inclination angle of 38^o to the center line.

6. Incremental values of pitching-moment coefficient obtained for negatively deflected elevons were unaffected by the presence of the tank at angles of attack below 15^o. There-

fore, in future separation studies, elevon-effectiveness parameters for the isolated orbiter may be used with reasonable confidence.

Langley Research Center,
National Aeronautics and Space Administration,
Hampton, Va., February 21, 1975.

REFERENCES

1. Stone, Howard W.: Supersonic and Hypersonic Aerodynamic Characteristics of Two Shuttle-Orbiter Configurations Designed for Reduced Length. NASA TM X-71956, 1974.

2. Decker, John P.; and Gera, Joseph: An Exploratory Study of Parallel-Stage Separation of Reusable Launch Vehicles. NASA TN D-4765, 1968.

3. Schaefer, William T., Jr.: Characteristics of Major Active Wind Tunnels at the Langley Research Center. NASA TM X-1130, 1965.

TABLE I.- GEOMETRIC CHARACTERISTICS OF MODELS AND REFERENCE DIMENSIONS

Orbiter:	
Fuselage:	
Nose radius, cm (in.)	0.50 (0.20)
Distance from nose to body-flap trailing edge, cm (in.)	22.31 (8.783)
Distance from nose to body-flap hinge line, cm (in.)	21.05 (8.288)
Wing:	
Root chord, cm (in.)	13.97 (5.50)
Tip chord, cm (in.)	2.00 (0.79)
Taper ratio	0.143
Aspect ratio	2.4
Dihedral angle, deg	7
Total planform area,* cm^2 (in^2)	156.98 (24.33)
Mean aerodynamic chord,* cm (in.)	9.58 (3.77)
Span, cm (in.)	19.43 (7.65)
Incidence:	
At body, deg	2
At tip, deg	-3
Elevon area, cm^2 (in^2)	22.37 (3.47)
Airfoil sections:	
At root	NACA 0008-64
At tip	NACA 0012-64
Vertical tail:	
Root chord, cm (in.)	5.49 (2.16)
Tip chord, cm (in.)	2.54 (1.00)
Area, cm^2 (in^2)	22.47 (3.48)
Aspect ratio	1.39
Span, cm (in.)	5.59 (2.20)
Airfoil section	NACA 0012-64
Body flap:	
Chord, cm (in.)	1.26 (0.50)
Area, cm^2 (in^2)	10.19 (1.58)
Span, cm (in.)	8.11 (3.19)
Tank:	
Diameter, cm (in.)	4.95 (1.95)
Length,* cm (in.)	35.43 (13.95)
Maximum cross-sectional area,* cm^2 (in^2)	19.23 (2.98)
Base area, cm^2 (in^2)	6.63 (1.03)
Nose radius, cm (in.)	0.49 (0.19)

*Reference values.

TABLE II.- SUMMARY OF RELATIVE INCIDENCE ANGLES α_i

z/d	α_i, deg, for –		
	x/d = 0	x/d = 0.641	x/d = 1.282
0	0	0	0
.256	-5, 0, 5	-5, 0, 5	-5, 0, 5
.513	-5, 0, 5	-5, 0, 5	-5, 0, 5
1.026	-5, 0, 5, 10	-5, 0, 5, 10	-5, 0, 5, 10

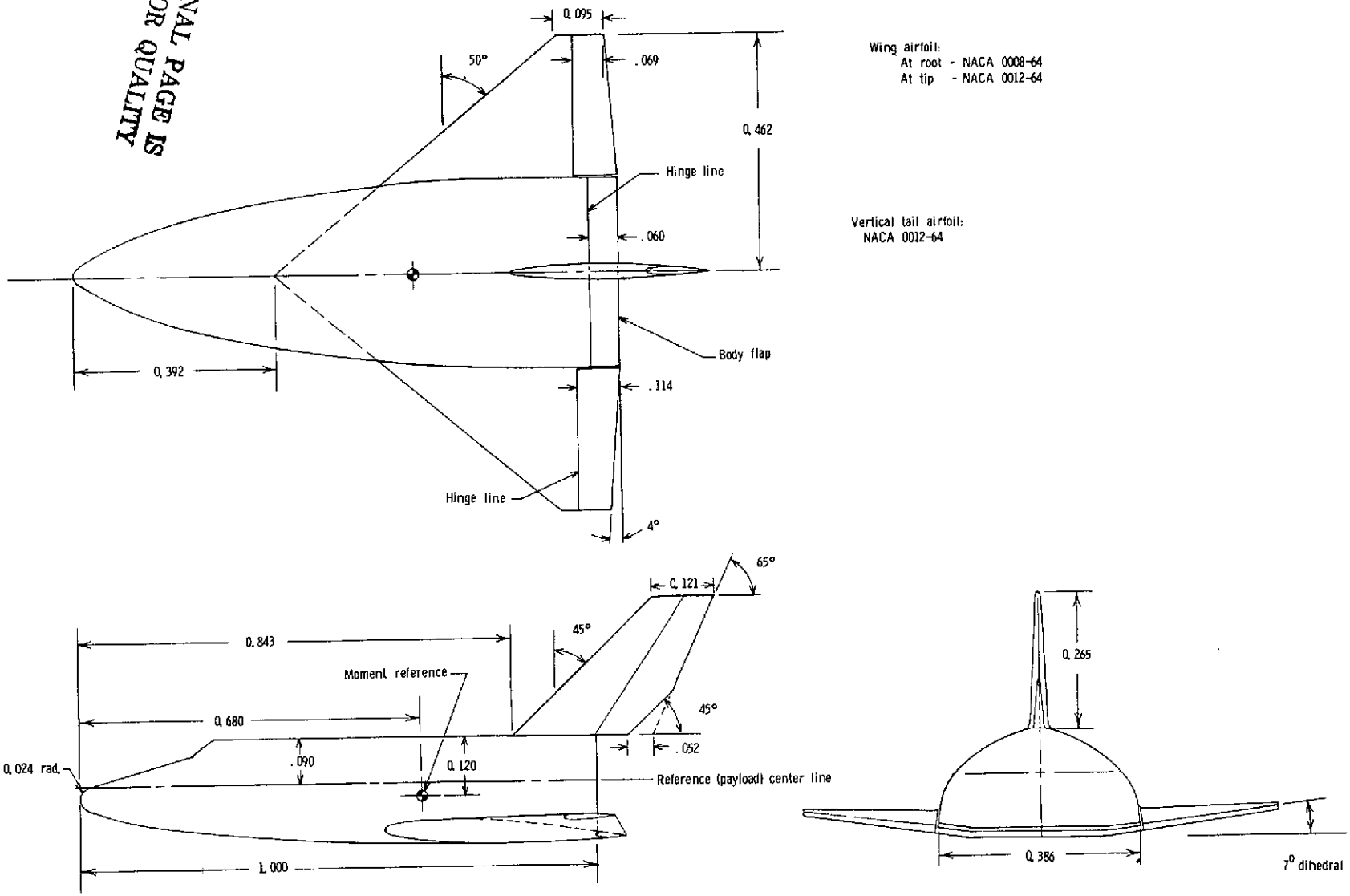

Figure 1.- Details of 0.0075-scale orbiter model. Dimensions are normalized by fuselage length, 21.05 cm (8.288 in.).

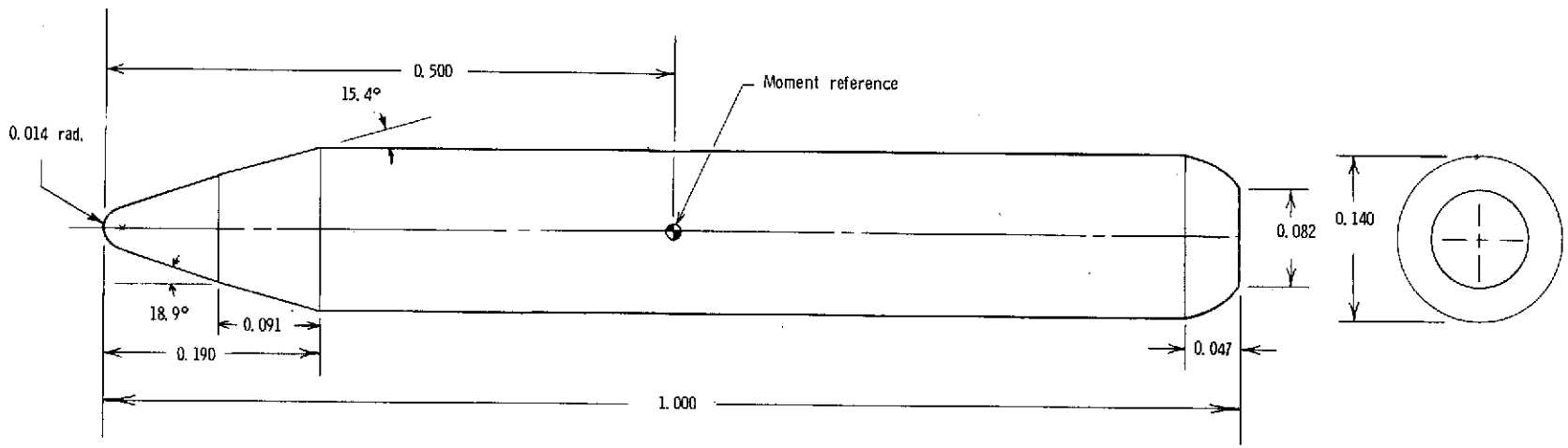

Figure 2.- Details of 0.0075-scale external tank. Dimensions are normalized by model length, 35.43 cm (13.95 in.).

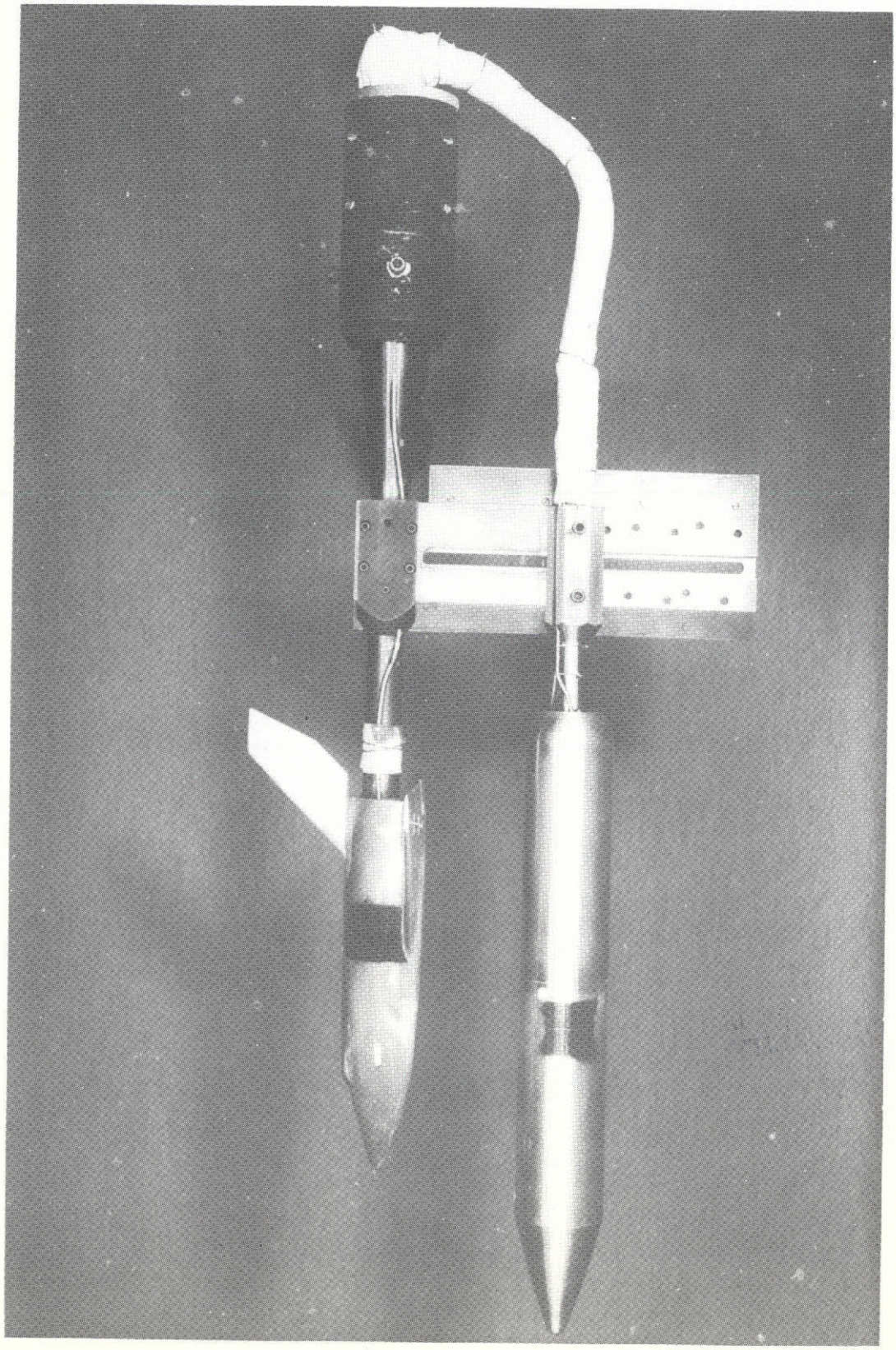

L-75-145

Figure 3.- Model-sting installation in tunnel test section.

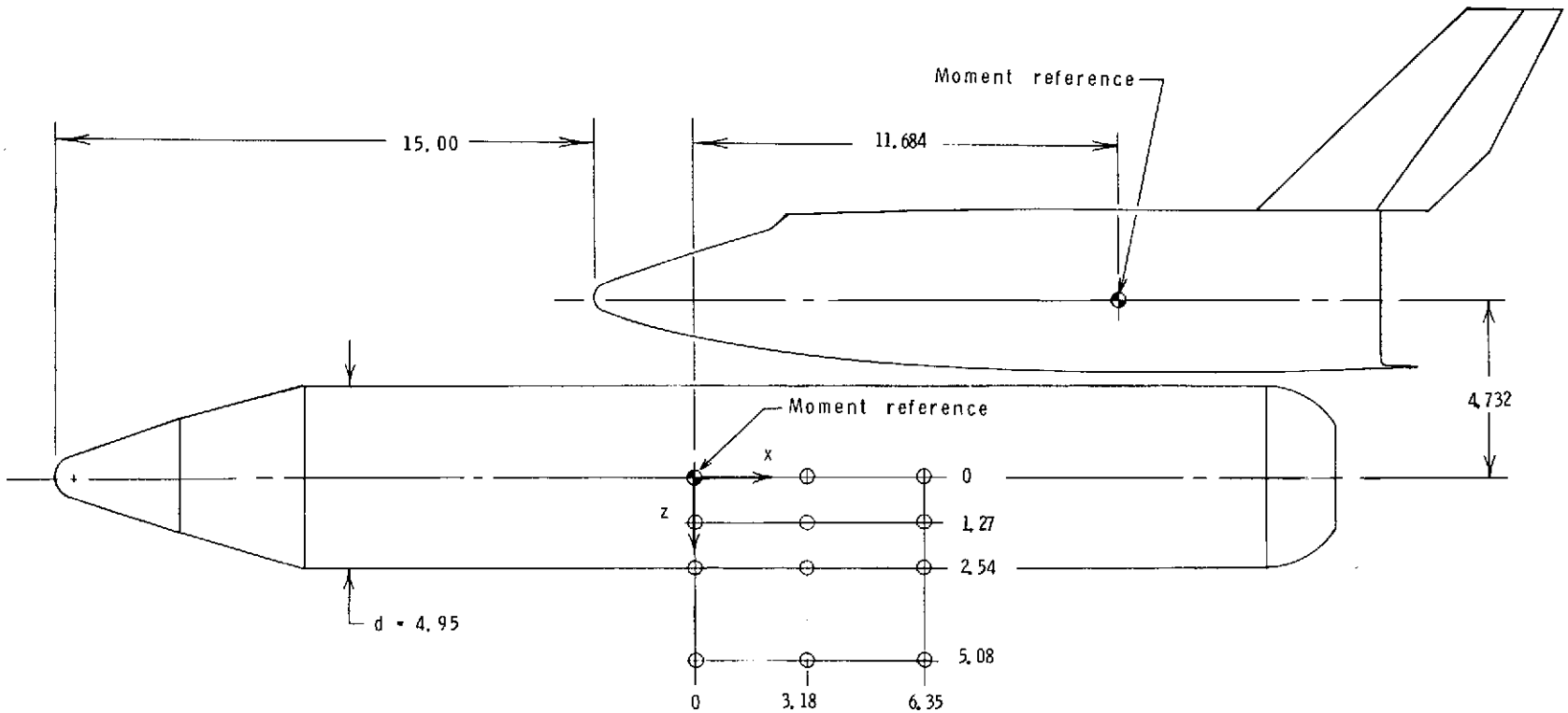

Location of tank model based on moment reference

x	x/d
0	0
3.18	0.641
6.35	1.282

z	z/d
0	0
1.27	0.256
2.54	0.513
5.08	1.026

Figure 4.- Grid layout used in separation tests. Models are shown in mated position with $\alpha_i = 0^o$. Dimensions are in centimeters.

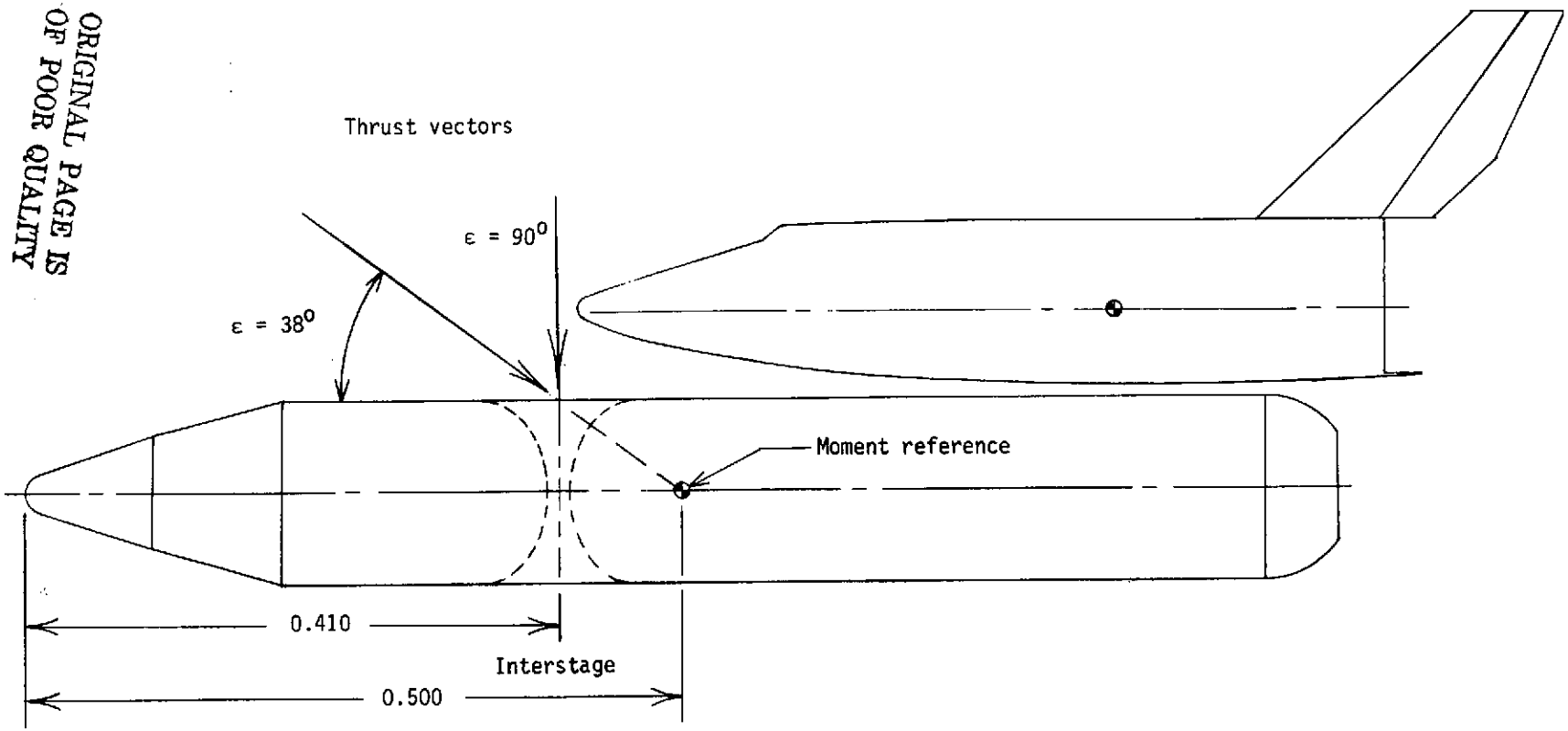

Figure 5.- Orientation of assumed thrust vectors applied to tank. Dimensions are normalized by tank length, 35.43 cm (13.95 in.).

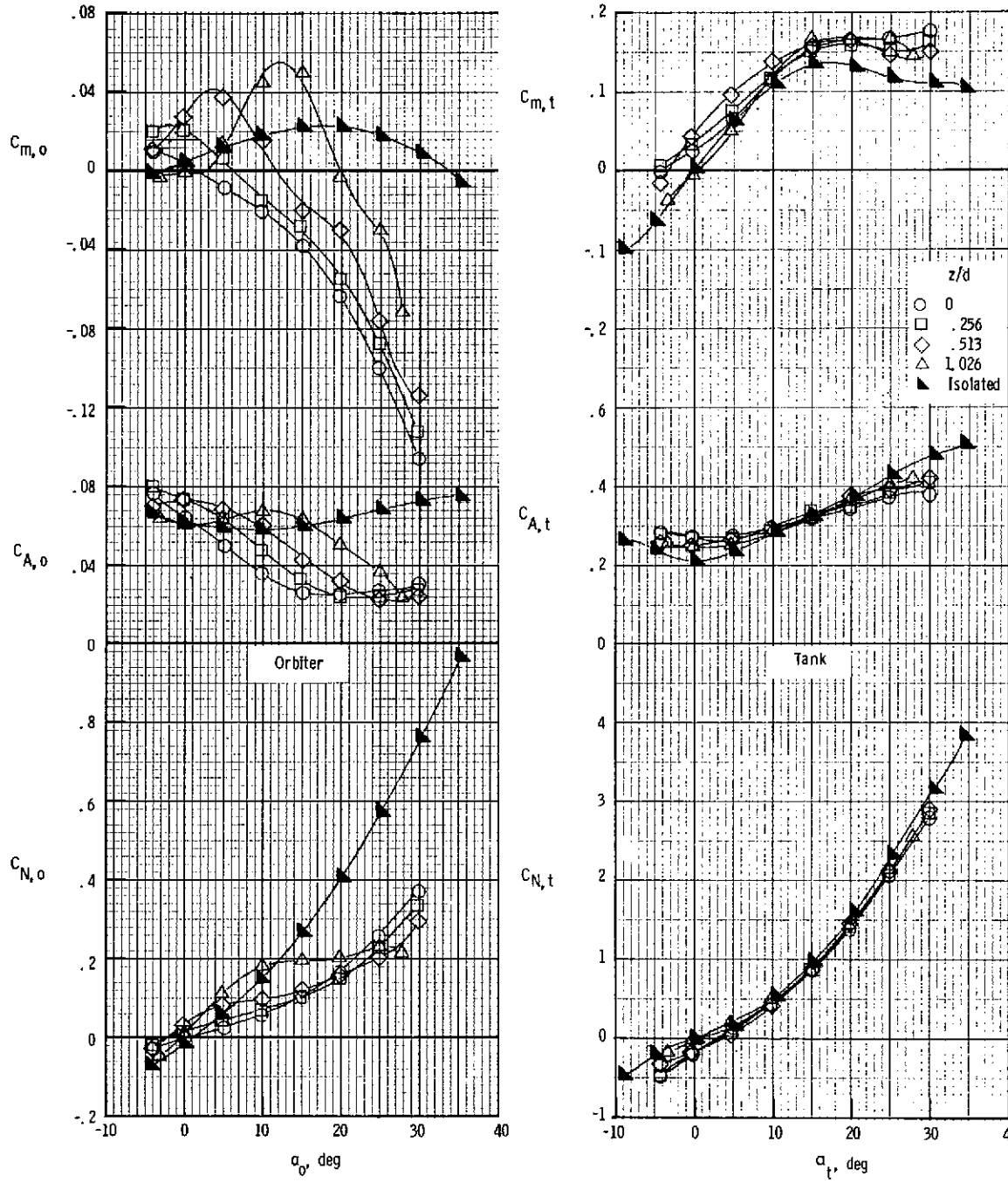

(a) x/d = 0.

Figure 6.- Effects of vertical spacing $\delta_e = 0^o$; $\alpha_i = 0^o$.

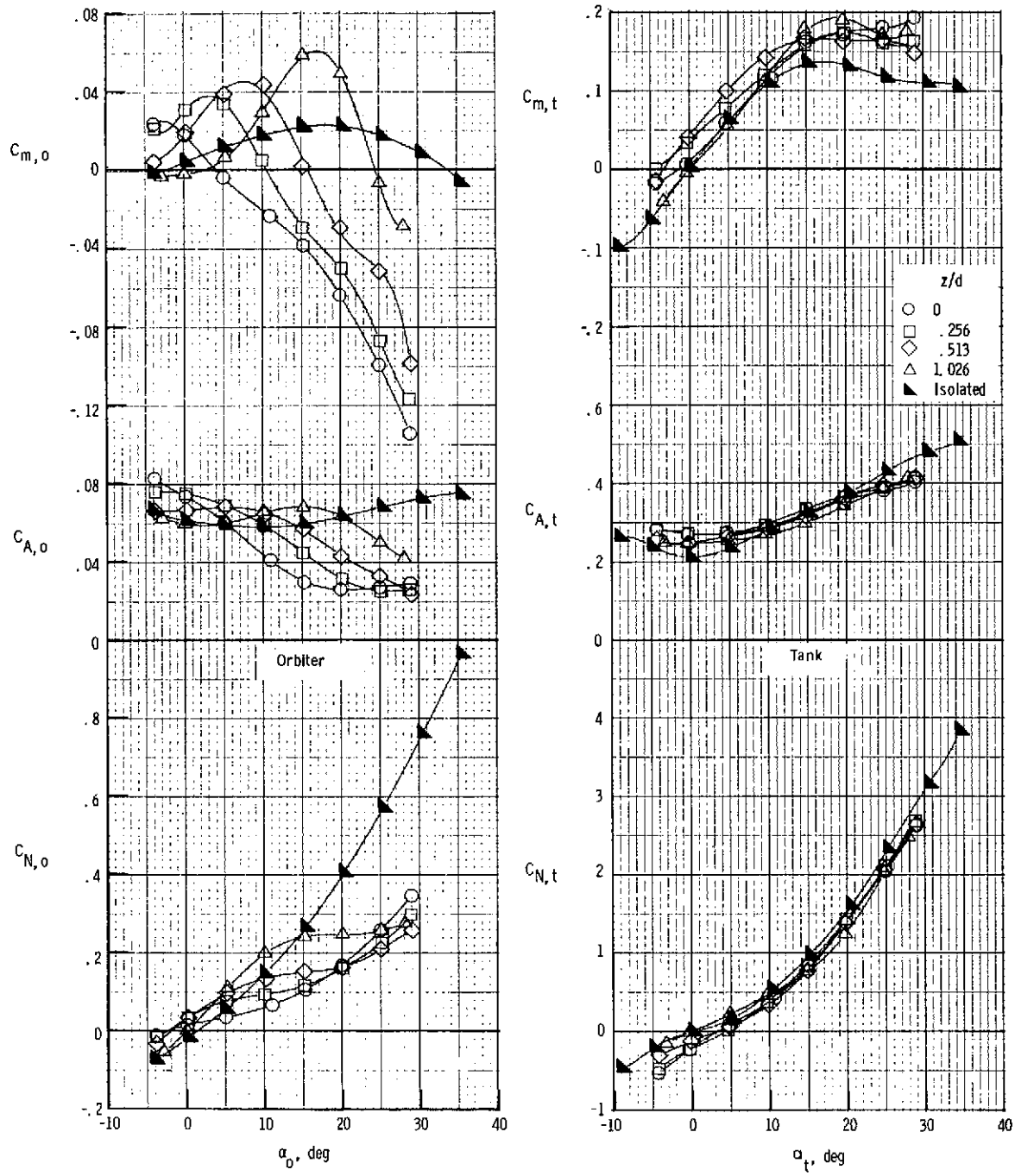

(b) x/d = 0.641.

Figure 6.- Continued.

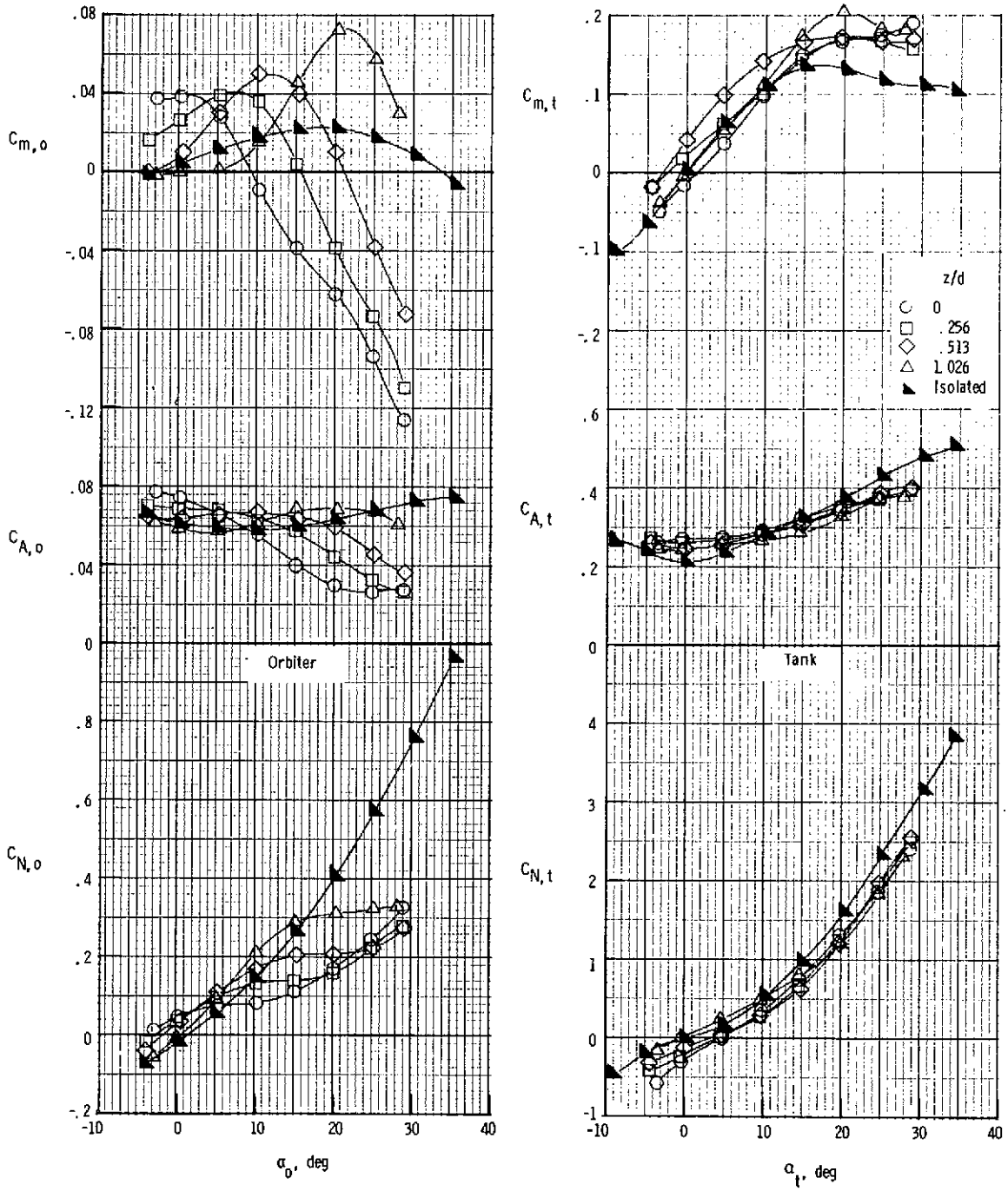

(c) x/d = 1.282.

Figure 6.- Concluded.

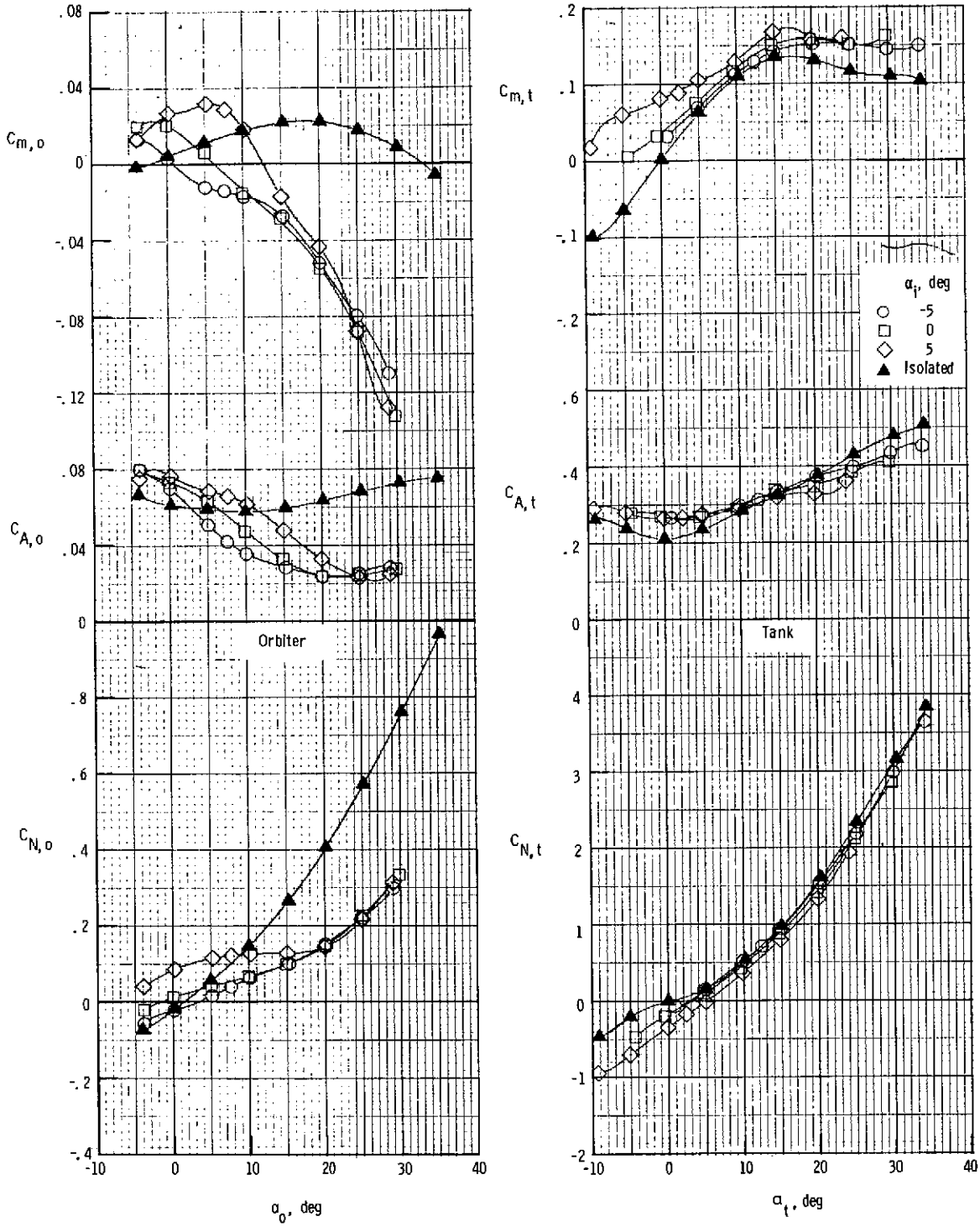

(a) x/d = 0.

Figure 7.- Effects of incidence angle at z/d = 0.256. $\delta_e = 0^o$.

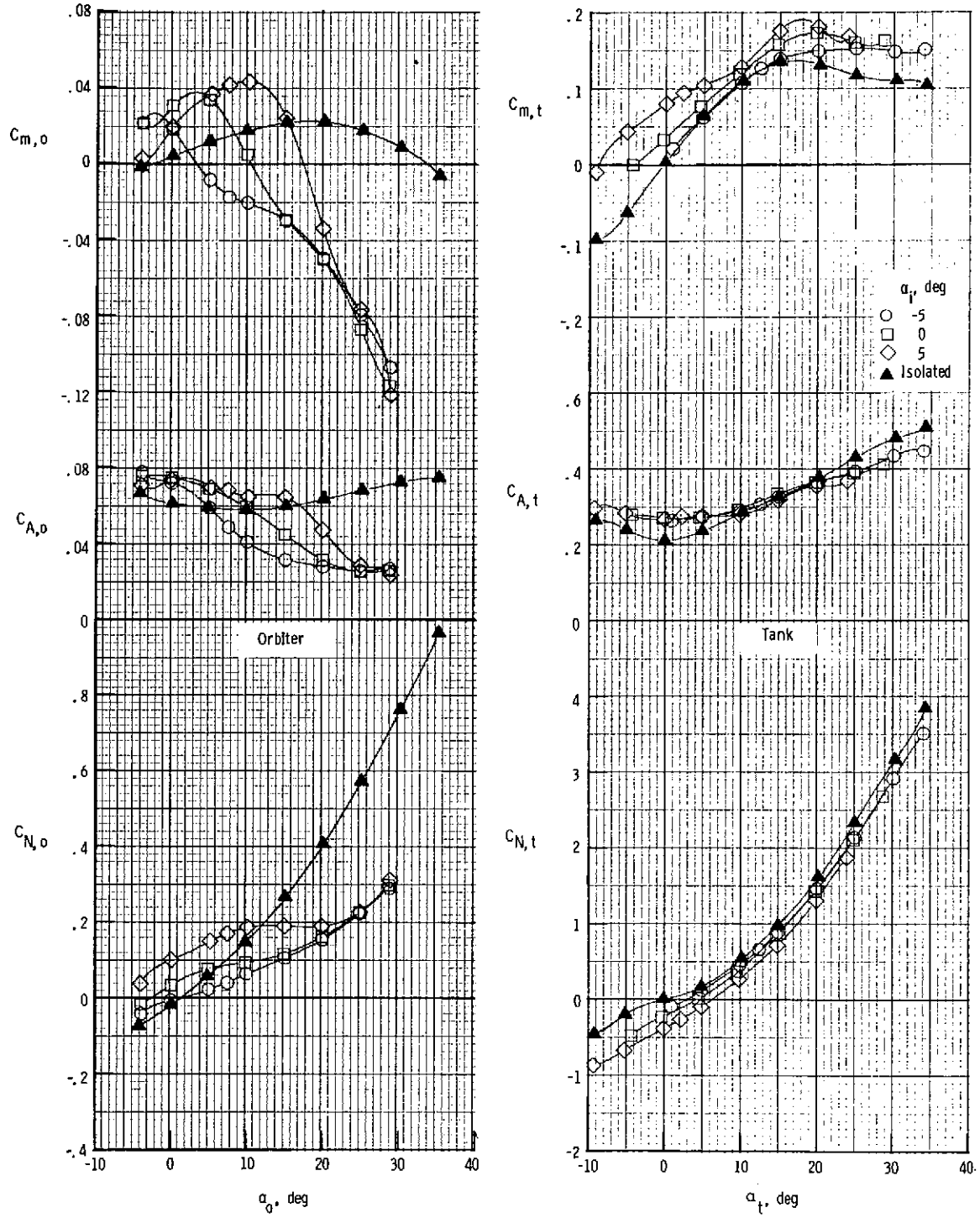

(b) x/d = 0.641.

Figure 7.- Continued.

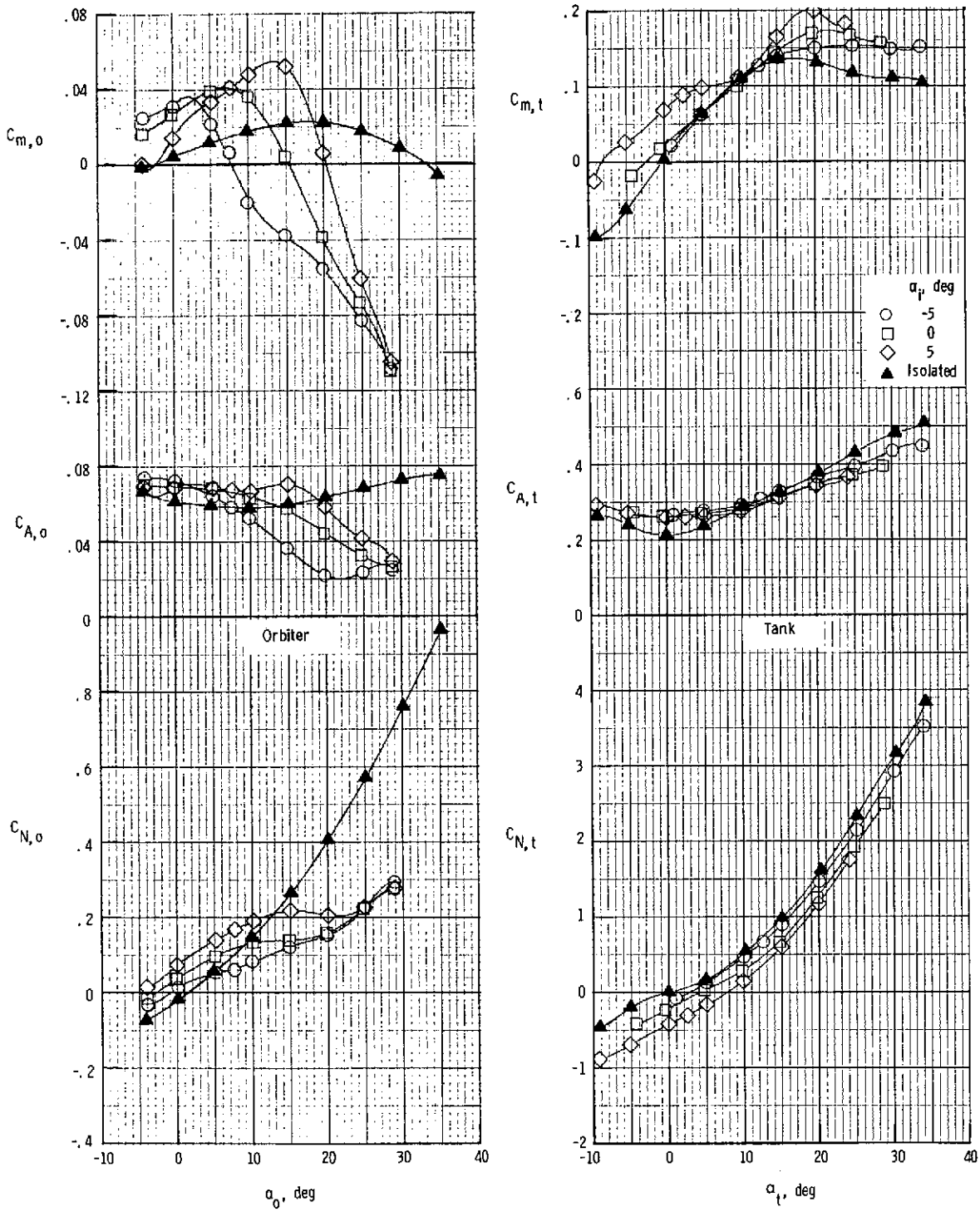

(c) x/d = 1.282.

Figure 7.- Concluded.

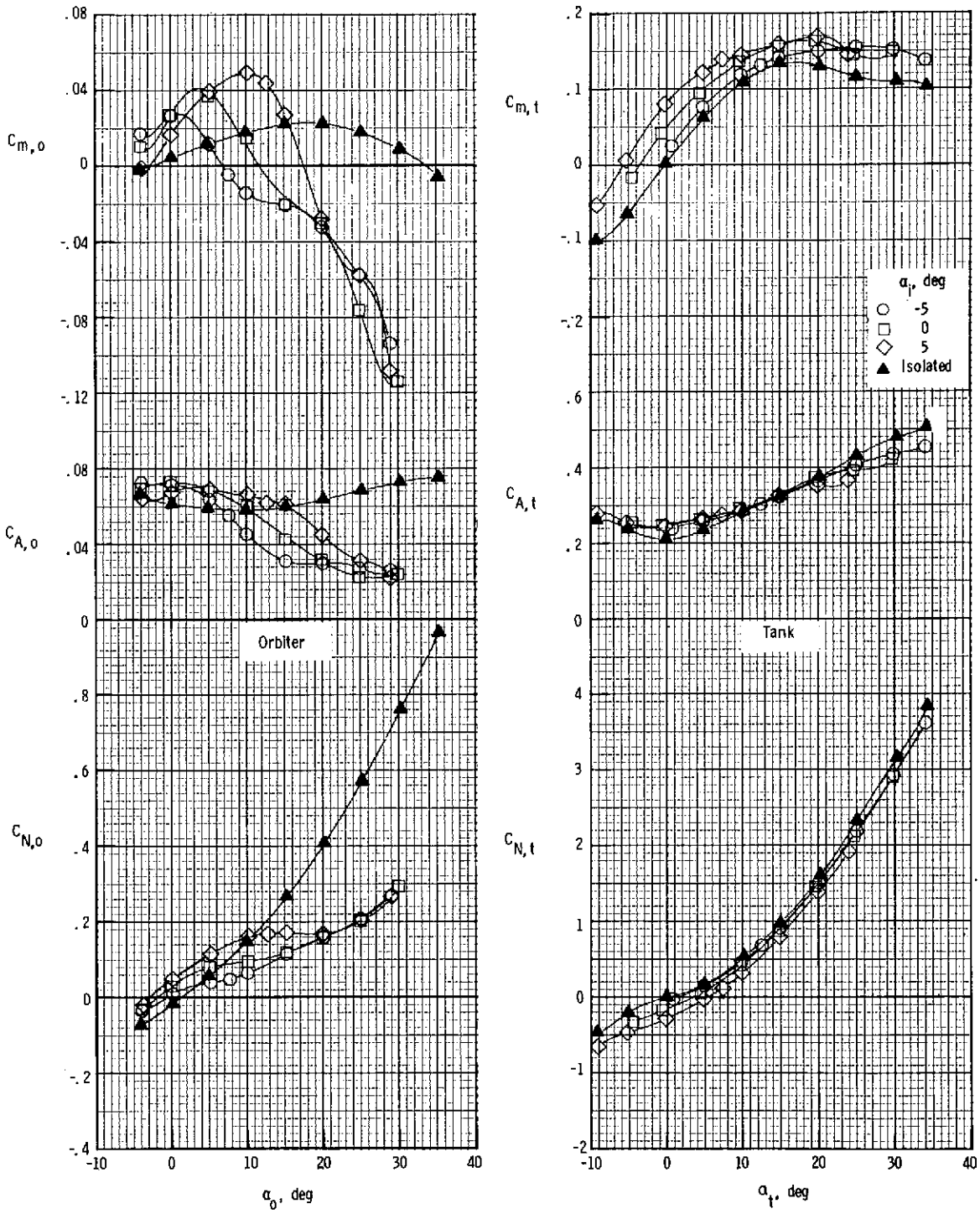

(a) x/d = 0.

Figure 8.- Effects of incidence angle at z/d = 0.513. $\delta_e = 0^o$.

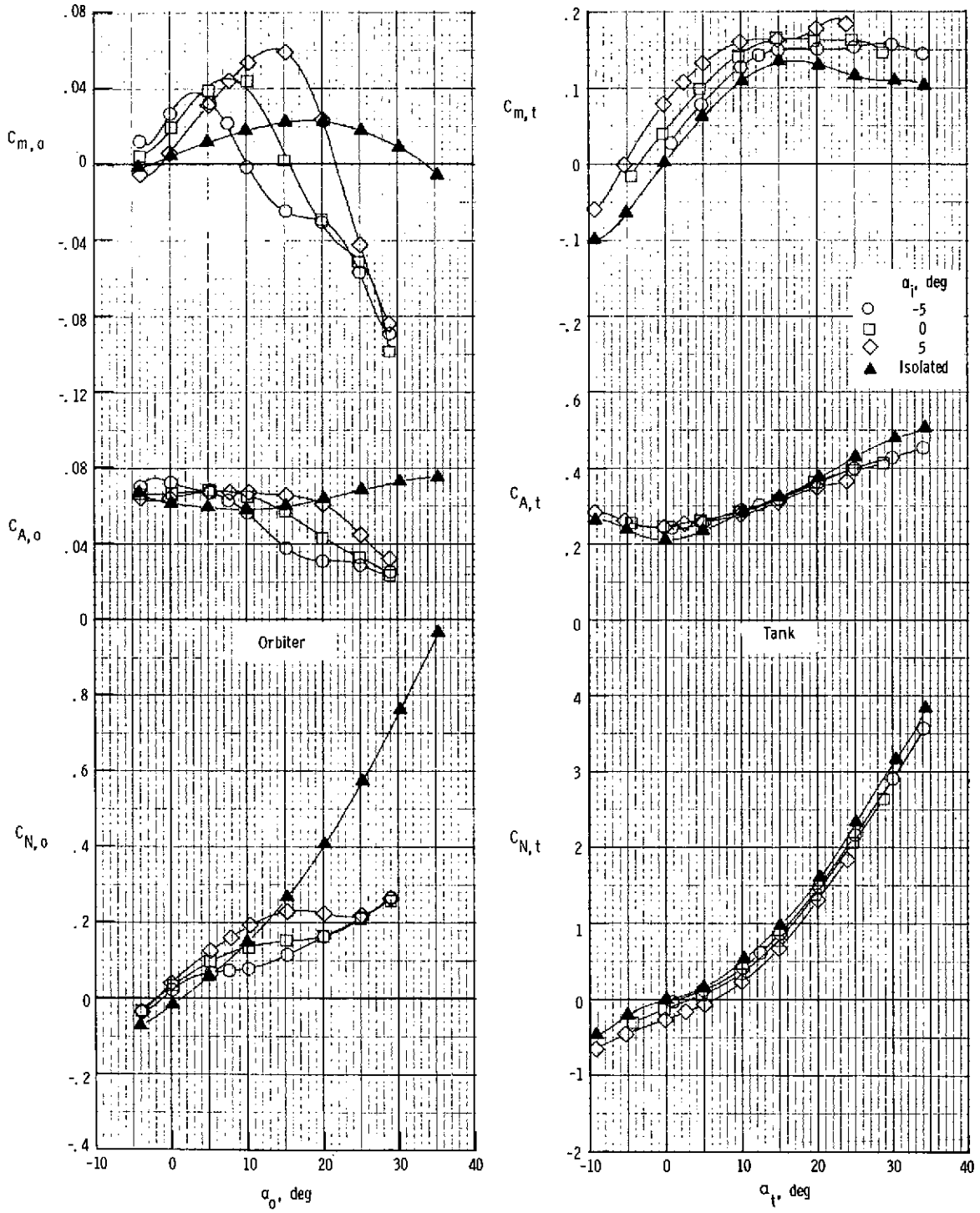

(b) x/d = 0.641.

Figure 8.- Continued.

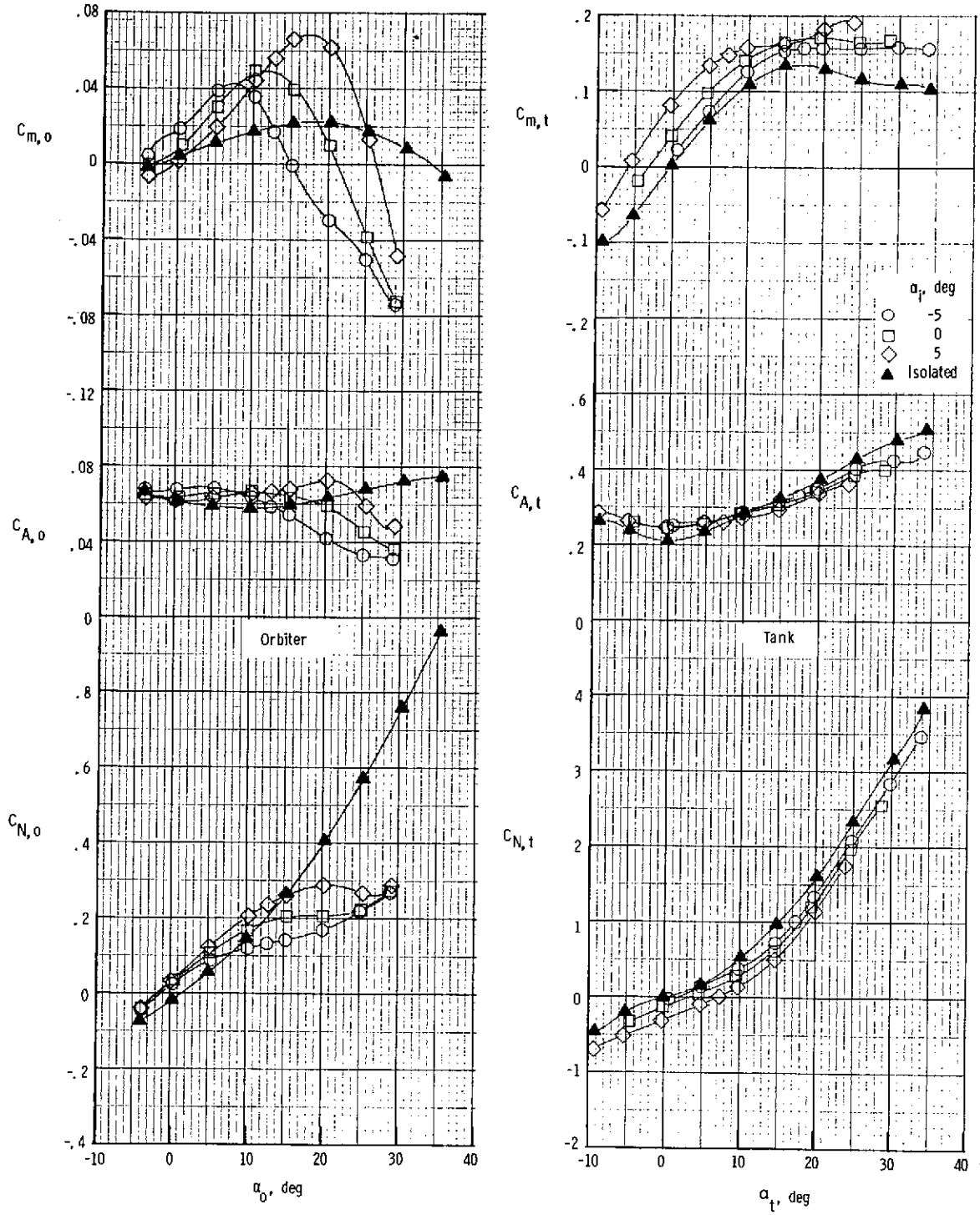

(c) x/d = 1.282.

Figure 8.- Concluded.

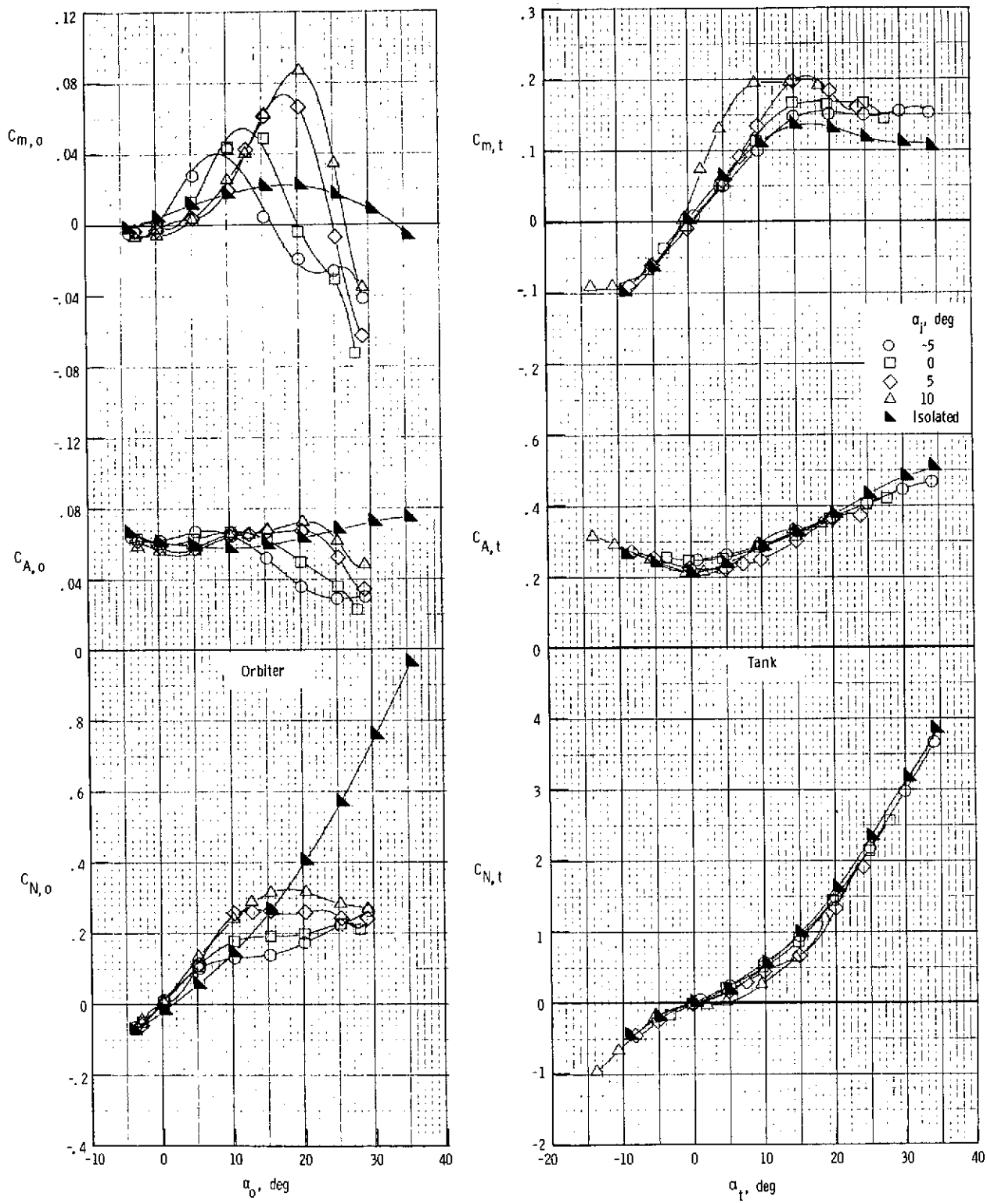

(a) x/d = 0.

Figure 9.- Effects of incidence angle at z/d = 1.026. $\delta_e = 0^o$.

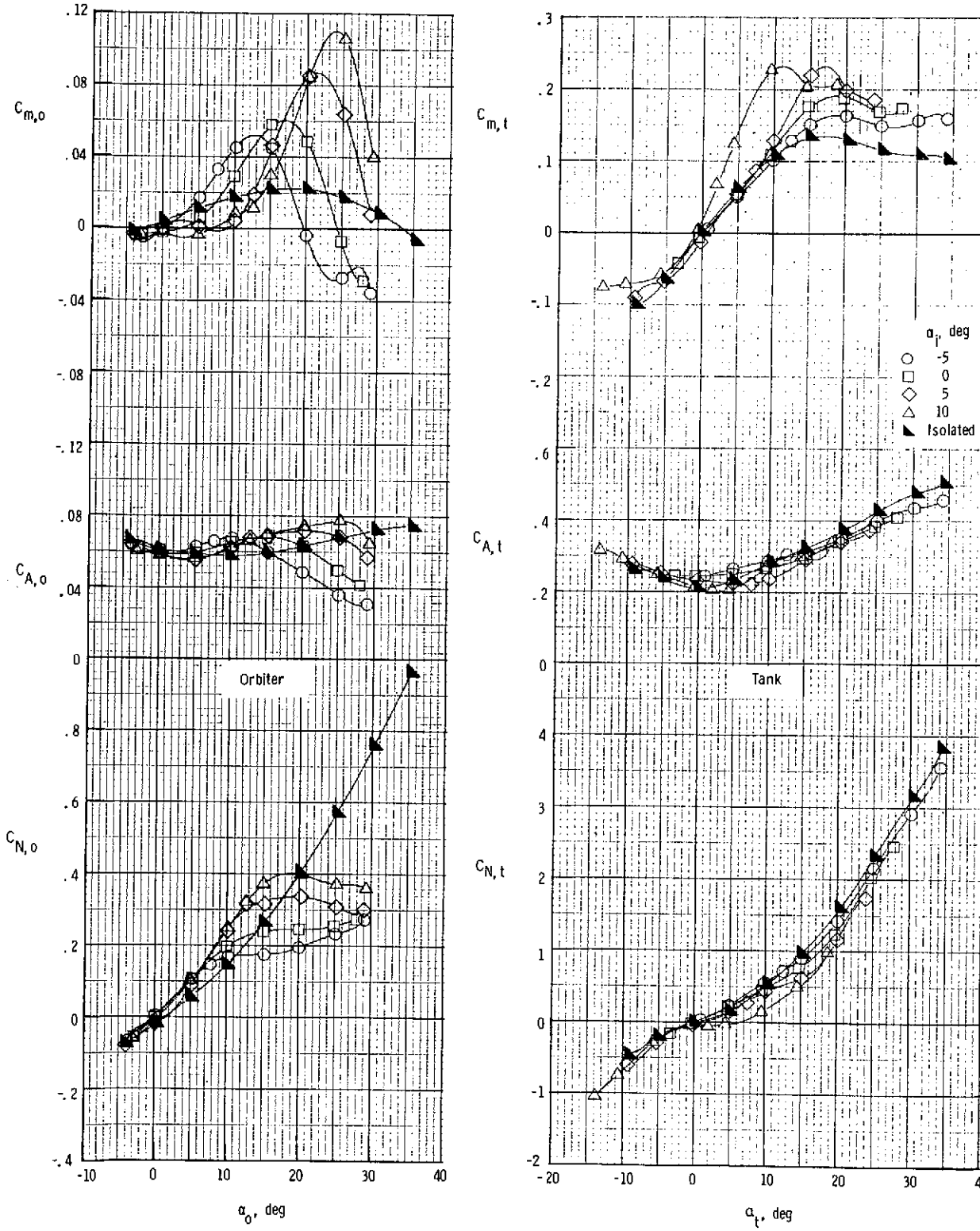

(b) x/d = 0.641.

Figure 9.- Continued.

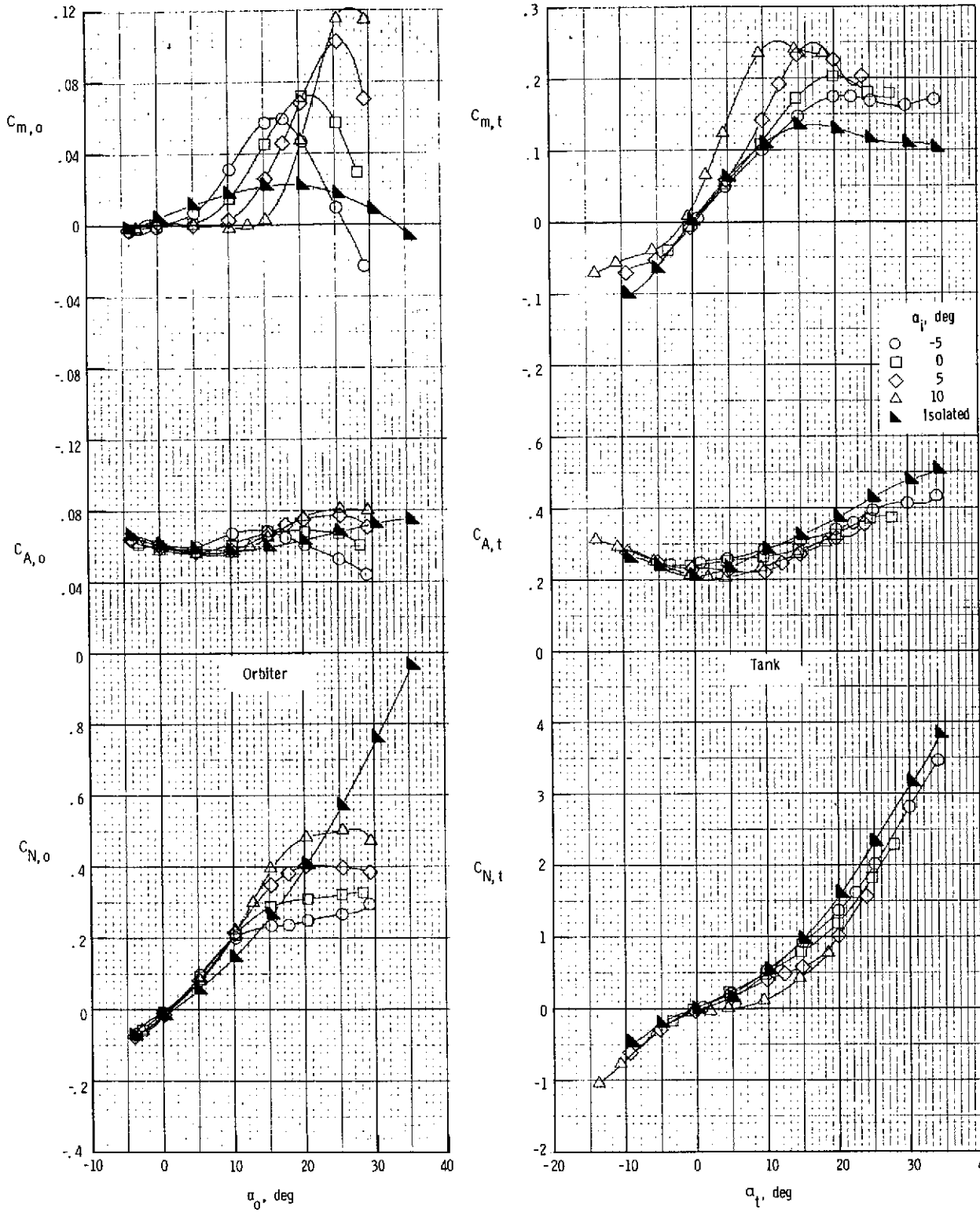

(c) x/d = 1.282.

Figure 9.- Concluded.

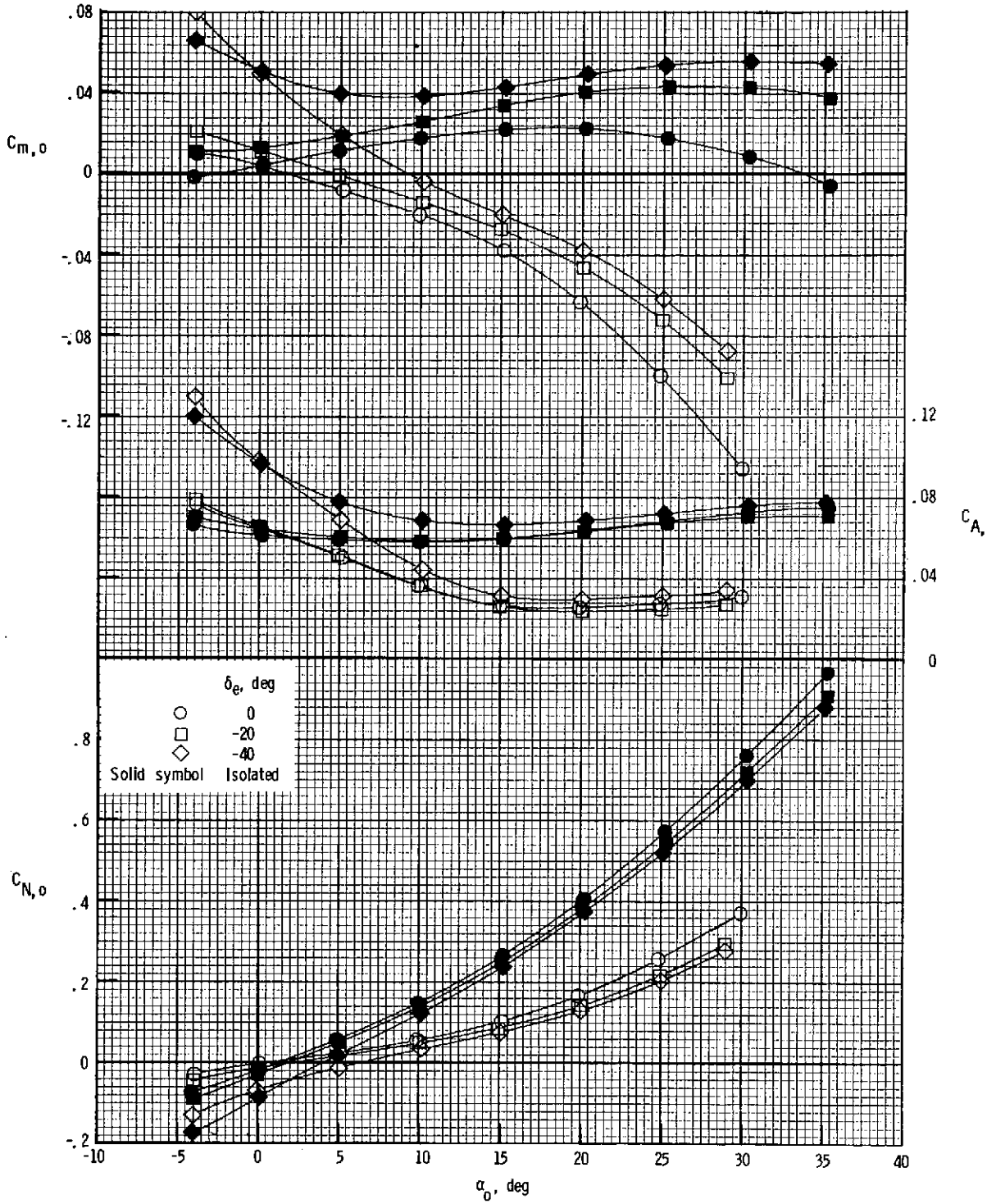

(a) x/d = 0; z/d = 0.

Figure 10.- Orbiter characteristics with elevon deflection in presence of tank. $\alpha_i = 0^o$.

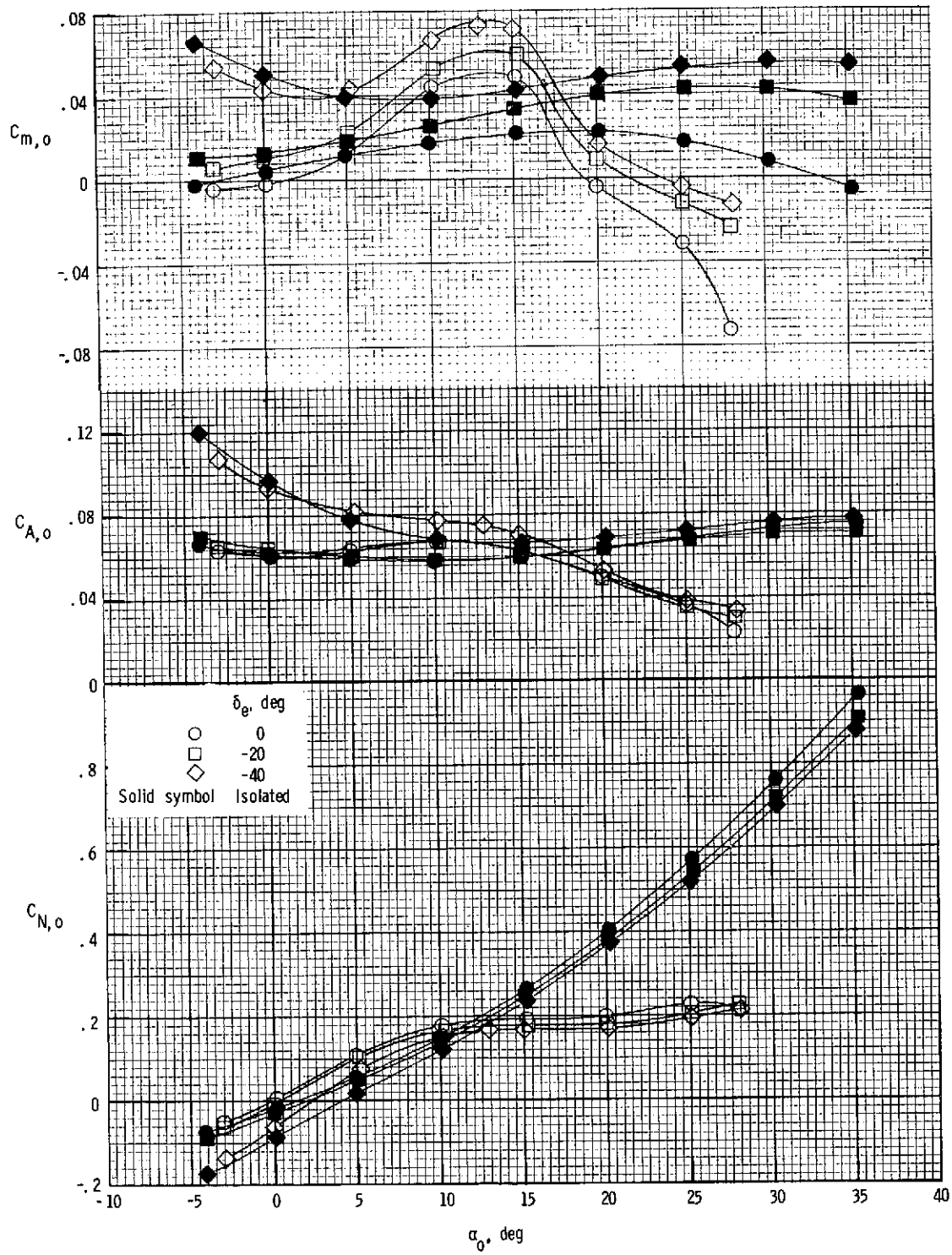

(b) x/d = 0; z/d = 1.026.

Figure 10.- Concluded.

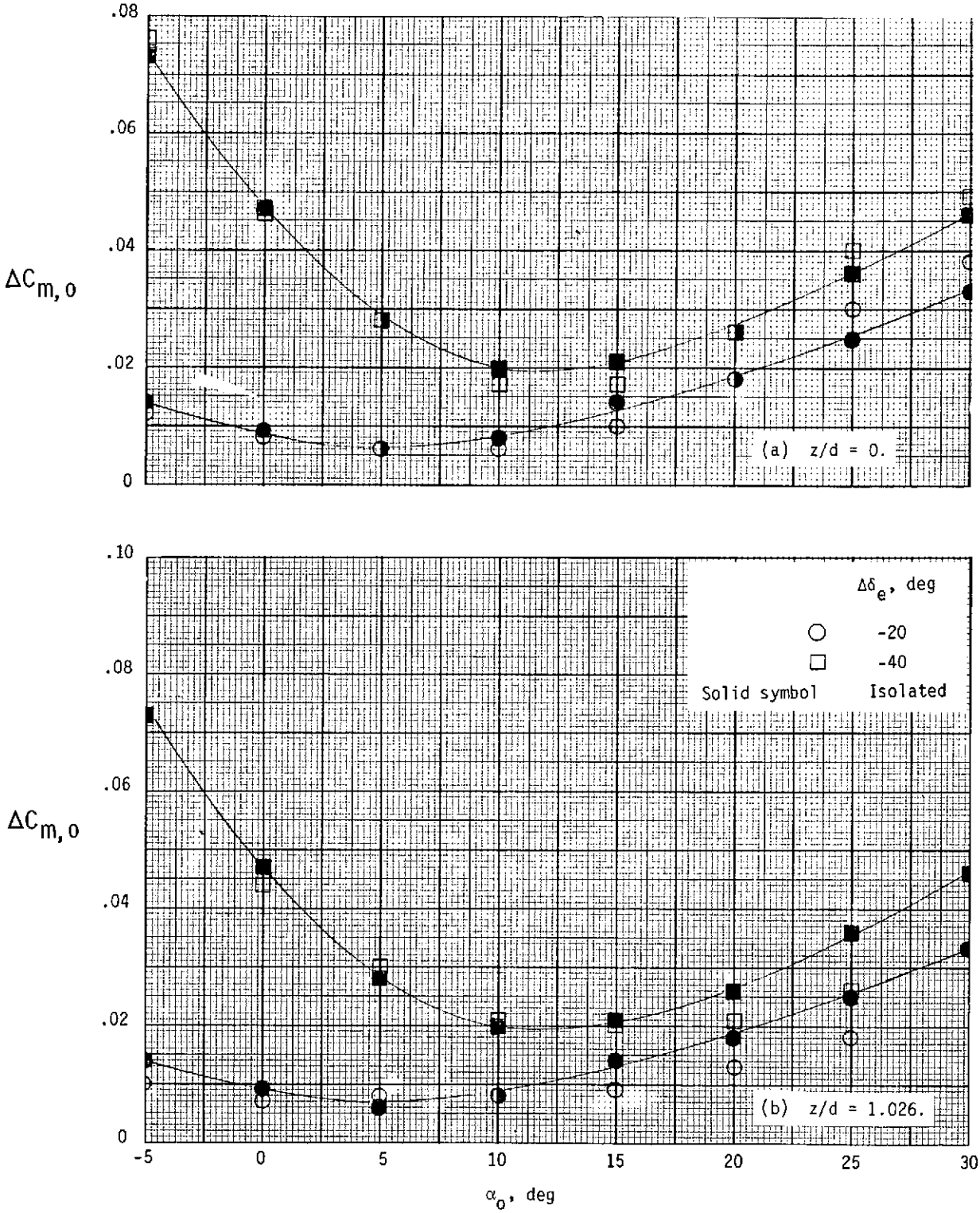

Figure 11.- Effects of tank interference on elevon effectiveness. $\alpha_i = 0^o$.

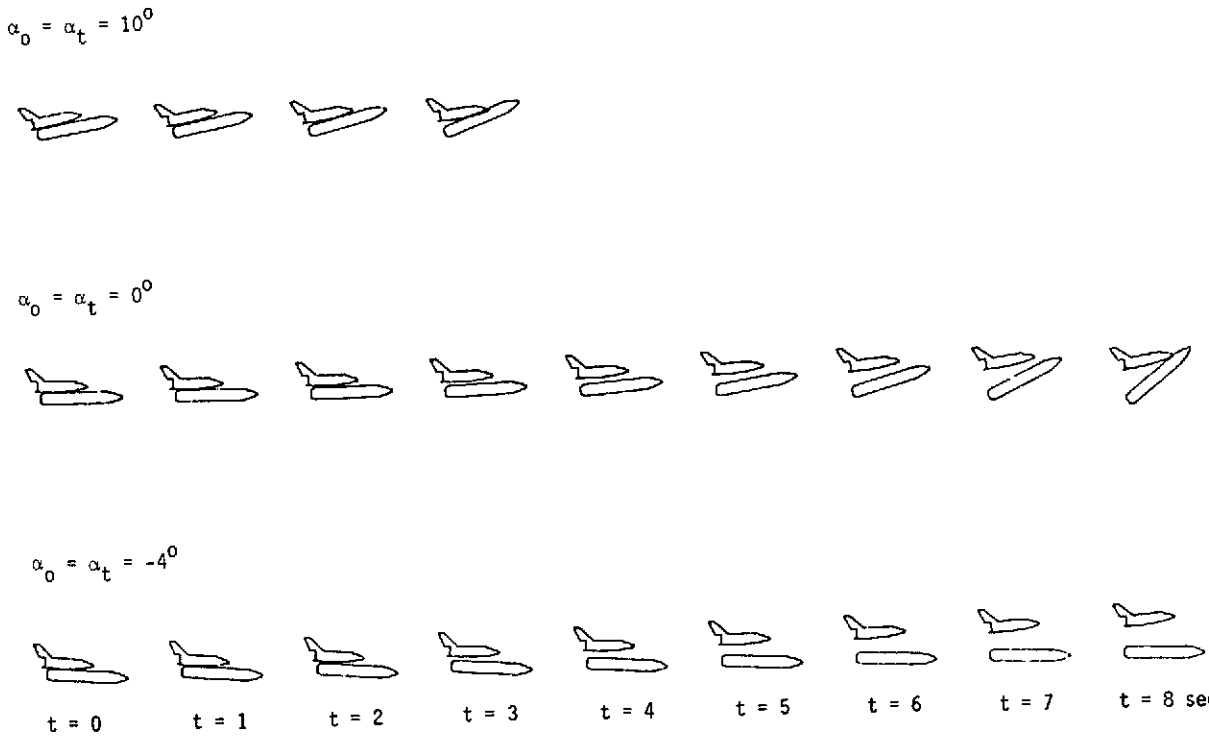

Figure 12.- Effects of initial angle of attack. $\delta_e = 0^o$; $\gamma = 0^o$; $q_\infty = 958$ N/m^2 (20 psf).

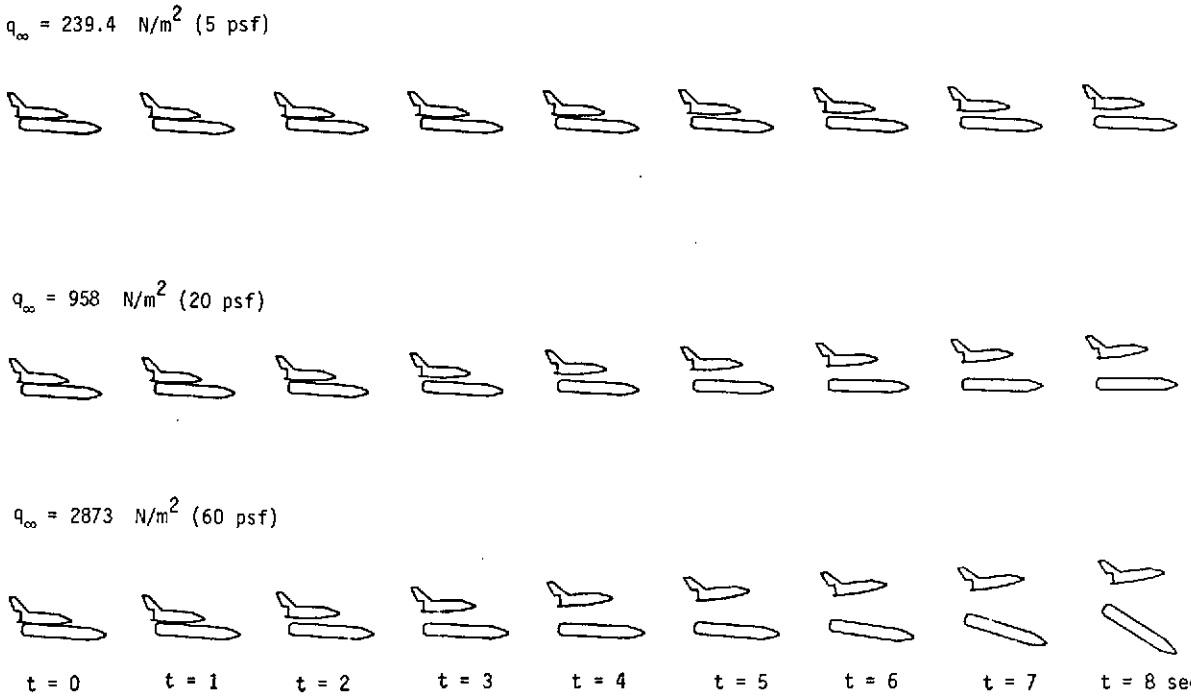

Figure 13.- Effects of dynamic pressure. $\alpha_o = \alpha_t = -4^o$ at $t = 0$; $\delta_e = 0^o$; $\gamma = 0^o$.

Figure 14.- Effects of initial flight-path angle. $\alpha_o = \alpha_t = -4^o$ at $t = 0$; $\delta_e = 0^o$; $q_\infty = 958$ N/m^2 (20 psf).

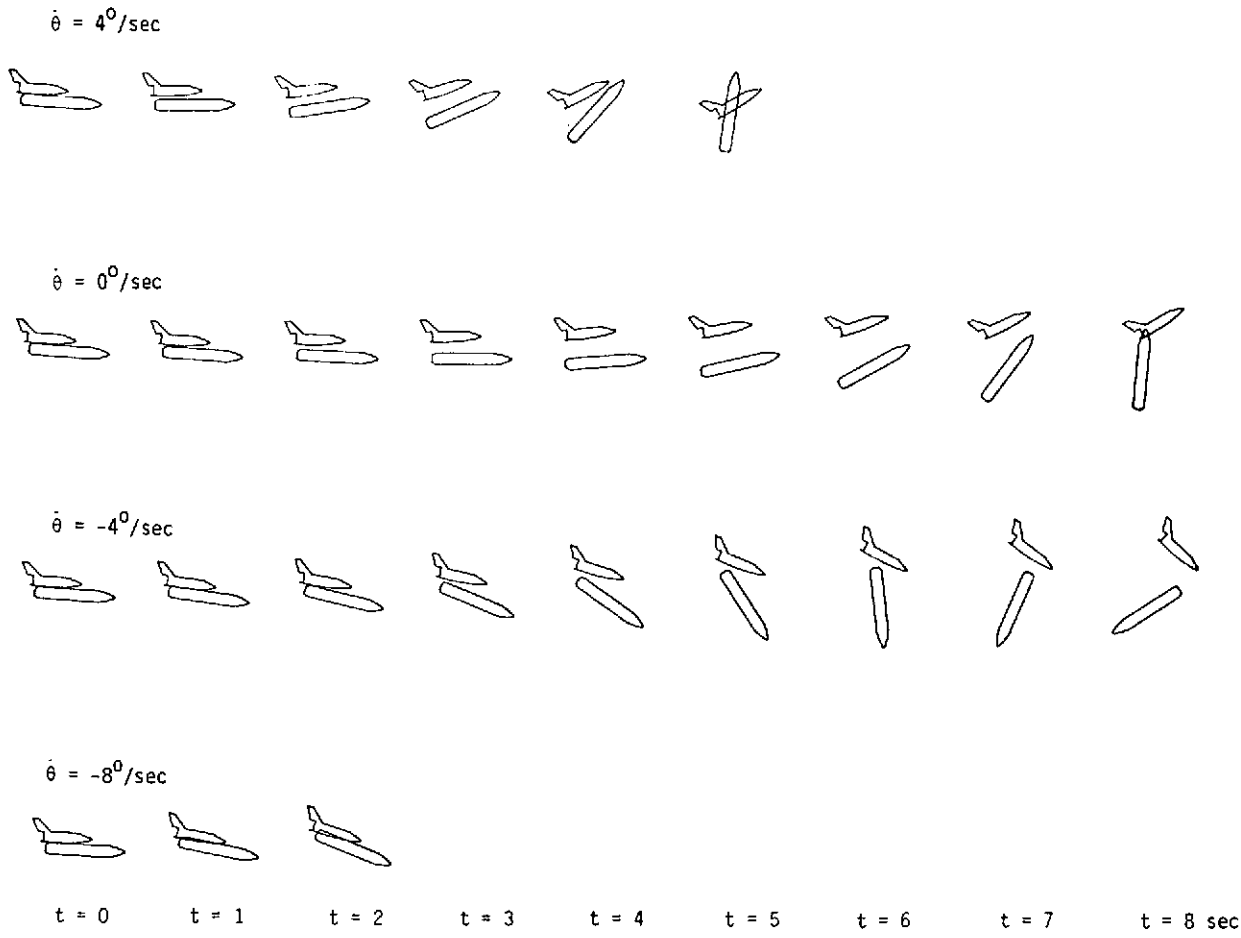

(a) $\alpha_o = \alpha_t = -3^o$ at $t = 0$.

Figure 15.- Effects of initial pitch rate. $\delta_e = 0^o$; $\gamma = 0^o$; $q_\infty = 2873$ N/m^2 (60 psf).

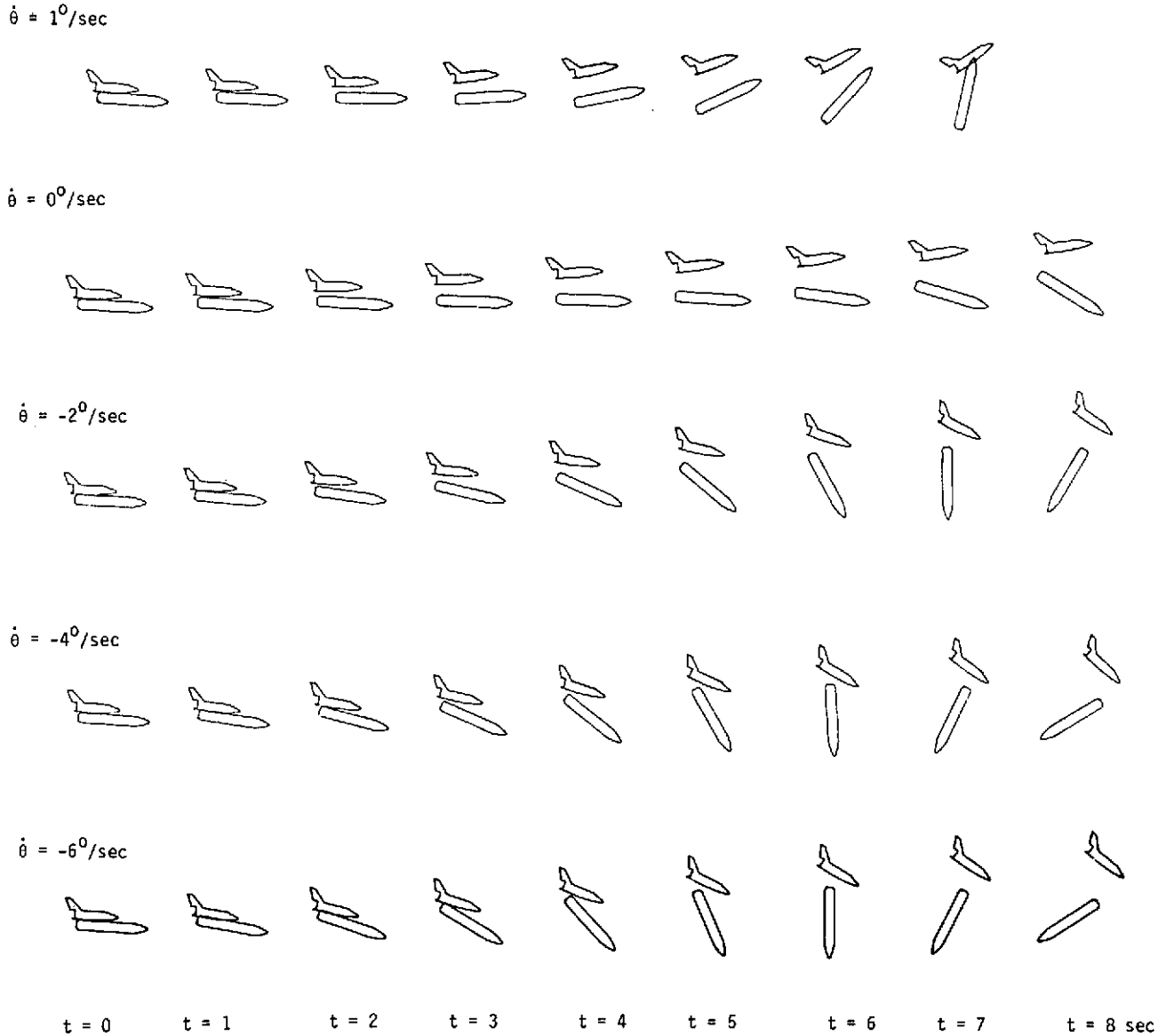

(b) $\alpha_o = \alpha_t = -4^o$ at $t = 0$.

Figure 15.- Continued.

(c) $\alpha_o = \alpha_t = -8^o$ at $t = 0$.

Figure 15.- Concluded.

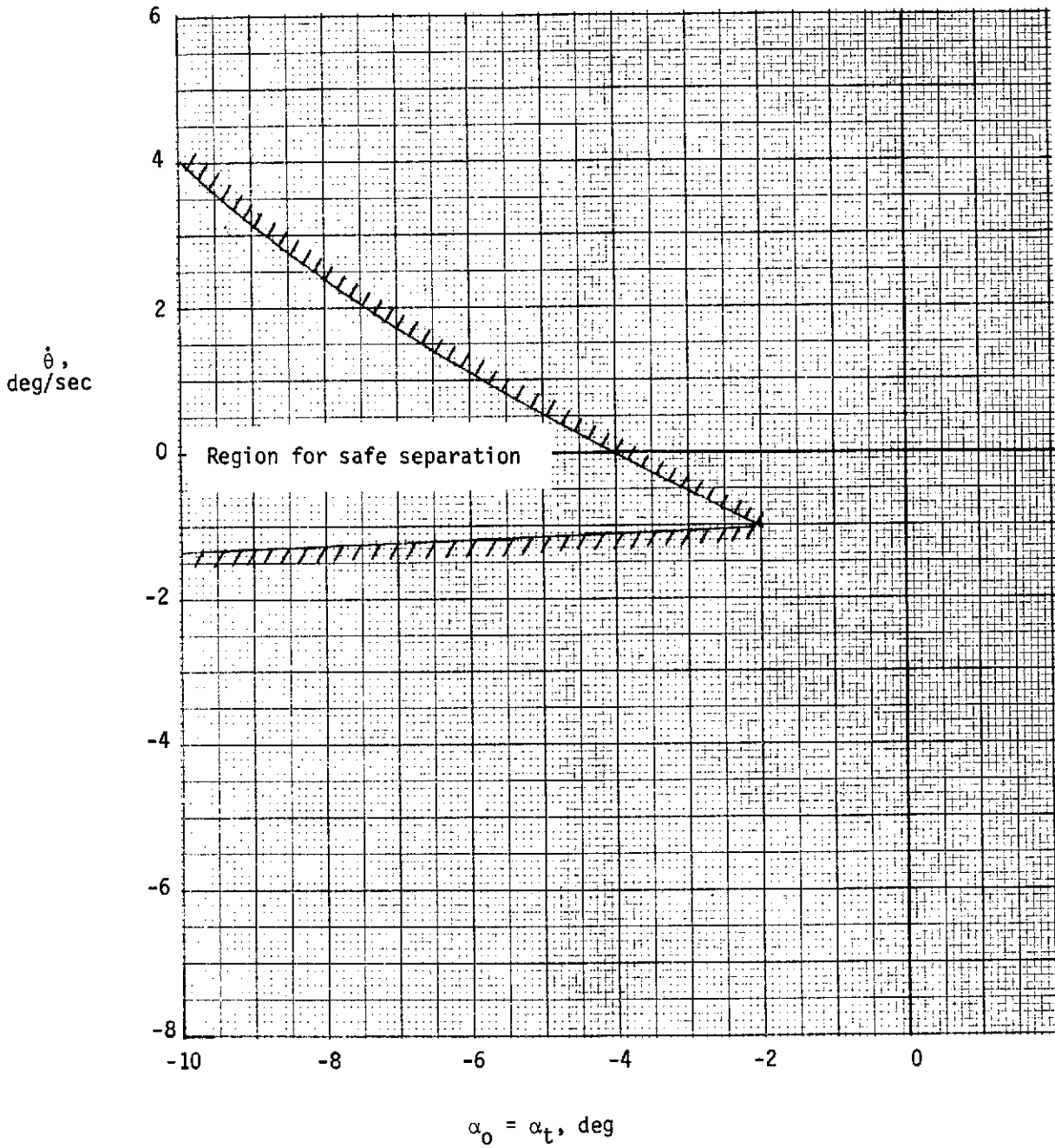

Figure 16.- Separation boundary for pitch rate as a function of angle of attack at t = 0 sec. q_∞ = 2873 N/m^2 (60 psf); $\delta_e = 0^o$; $\gamma = 0^o$.

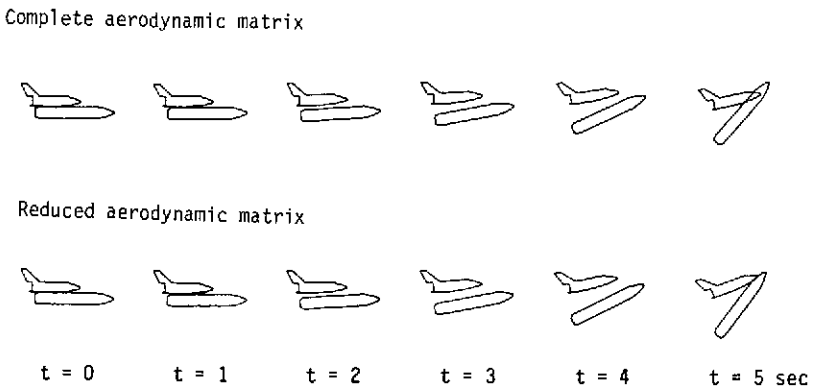

(a) $\alpha_o = \alpha_t = 0^o$ at $t = 0$.

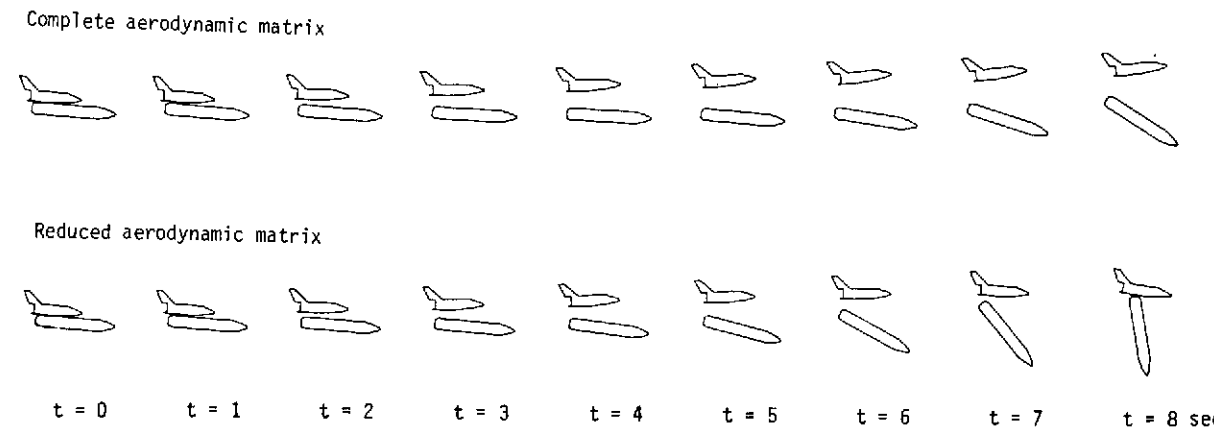

(b) $\alpha_o = \alpha_t = -4^o$ at $t = 0$.

Figure 17.- Effects of reduced aerodynamic matrix.
$\delta_e = 0^o$; $\gamma = 0^o$; $q_\infty = 2873$ N/m^2 (60 psf).

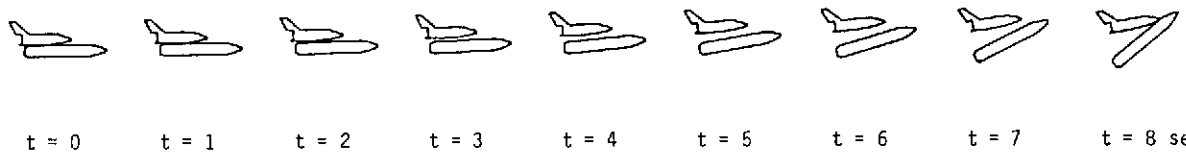

(a) No thrust. $\delta_e = 0^o$.

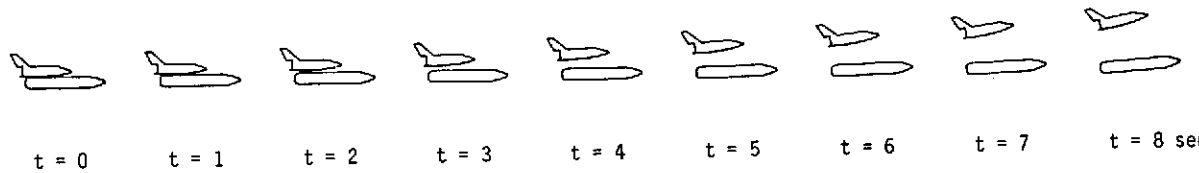

(b) $\epsilon = 90^o$; $\delta_e = 0^o$; thrust, 11.1 kN (2500 lb).

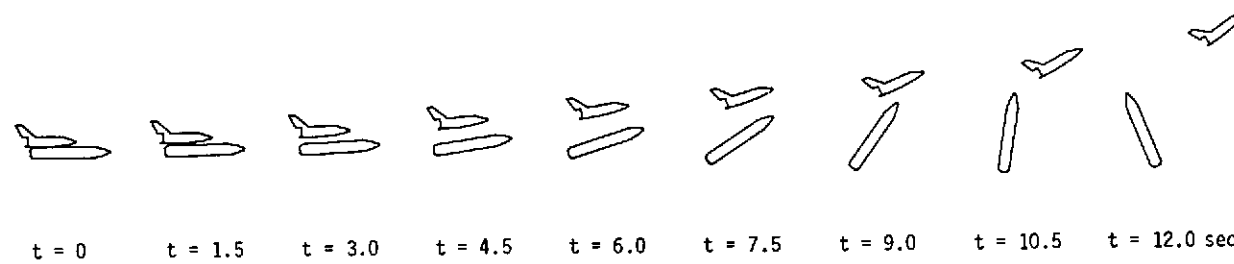

(c) $\epsilon = 38^o$; $\delta_e = 0^o$; thrust, 22.2 kN (5000 lb).

Figure 18.- Effects of thrust for $\alpha_o = \alpha_t = 0^o$ at t = 0.
$\gamma = 0^o$; $q_\infty = 958$ N/m^2 (20 psf).

(a) $\epsilon = 90^{o}$; $\delta_e = 0^{o}$; thrust, 43.1 kN (9700 lb).

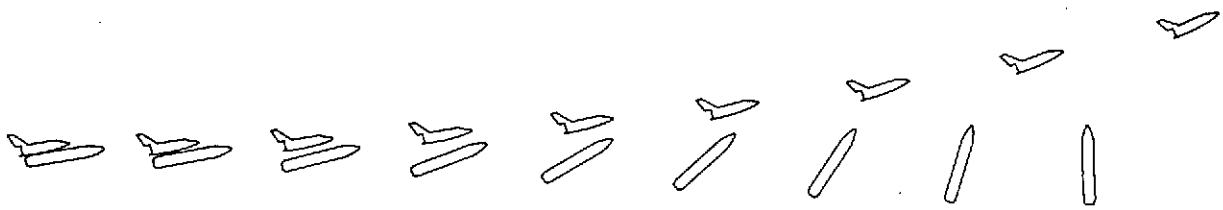

(b) $\epsilon = 38^{o}$; $\delta_e = -40^{o}$; thrust, 100 kN (22 500 lb).

Figure 19.- Effects of thrust for $\alpha_o = \alpha_t = 10^{o}$ at t = 0. $\gamma = 0^{o}$; $q_\infty = 958$ N/m^2 (20 psf).

(a) $\epsilon = 90^{o}$; $\delta_e = -40^{o}$; thrust, 60 kN (13 500 lb).

(b) $\epsilon = 38^{o}$; $\delta_e = -40^{o}$; thrust, 142.3 kN (32 000 lb).

Figure 20.- Effects of thrust for $\alpha_o = \alpha_t = 20^{o}$ at t = 0. $\gamma = 0^{o}$; $q_\infty = 958$ N/m^2 (20 psf).

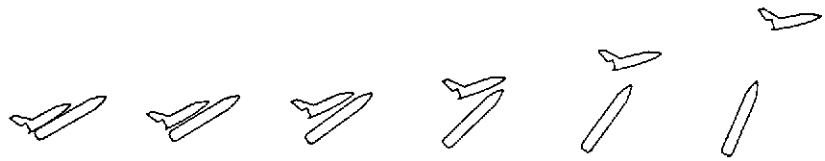

(a) $\epsilon = 90^{o}$; $\delta_e = -40^{o}$; thrust, 80 kN (18 000 lb).

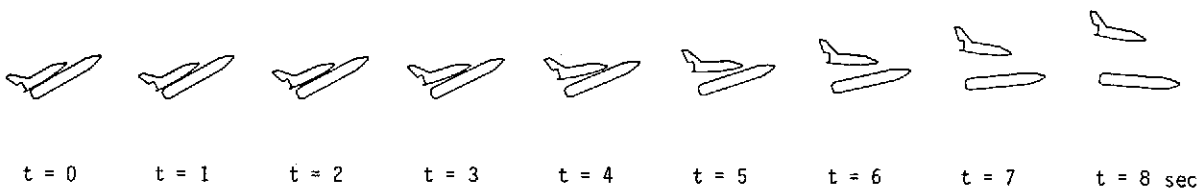

(b) $\epsilon = 38^{o}$; $\delta_e = -40^{o}$; thrust, 200 kN (45 000 lb).

Figure 21.- Effects of thrust for $\alpha_o = \alpha_t = 30^{o}$ at $t = 0$. $\gamma = 0^{o}$; $q_\infty = 958$ N/m2 (20 psf).

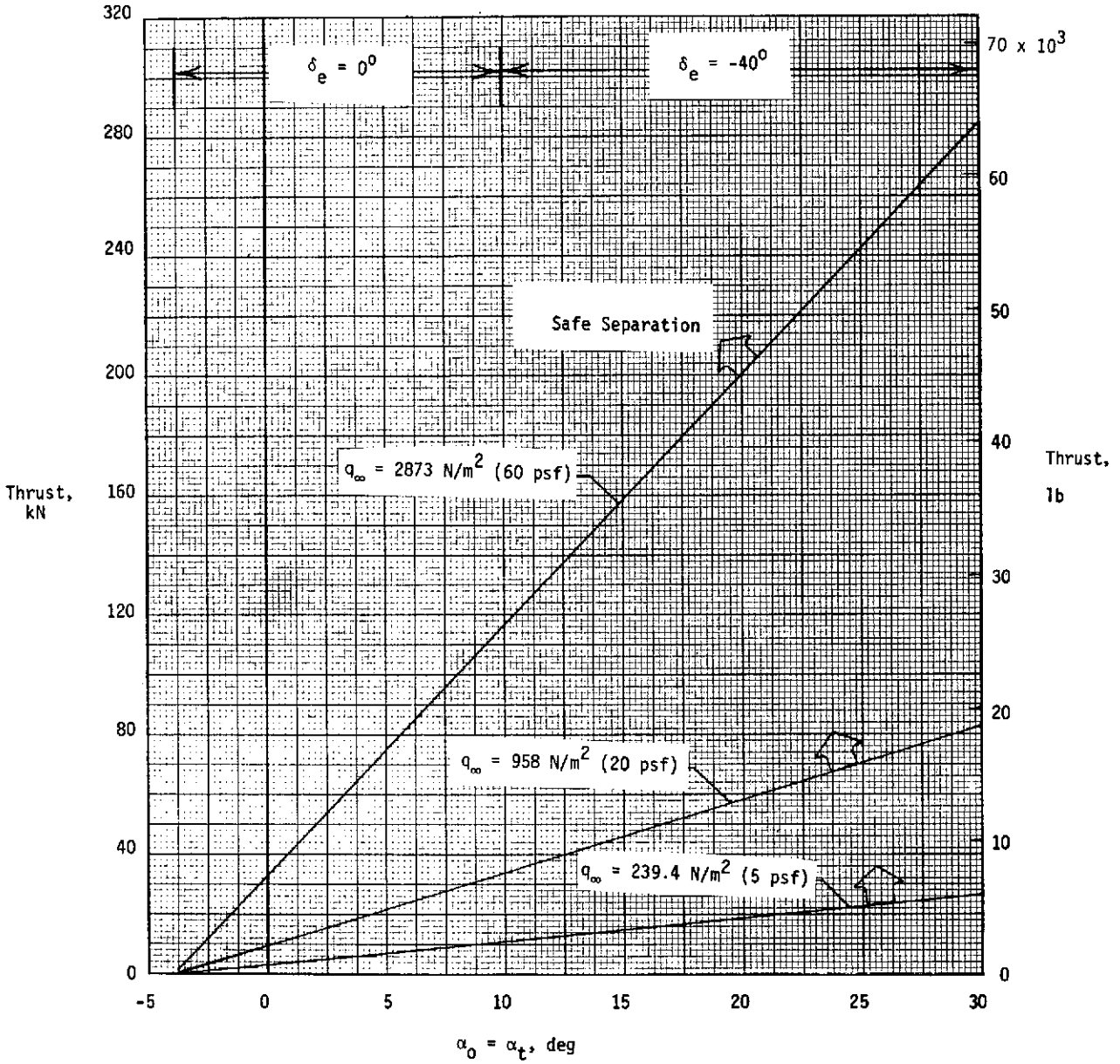

(a) $\epsilon = 90^o$.

Figure 22.- Separation boundaries for thrust as a function of angle of attack at t = 0 sec. $\gamma = 0^o$.

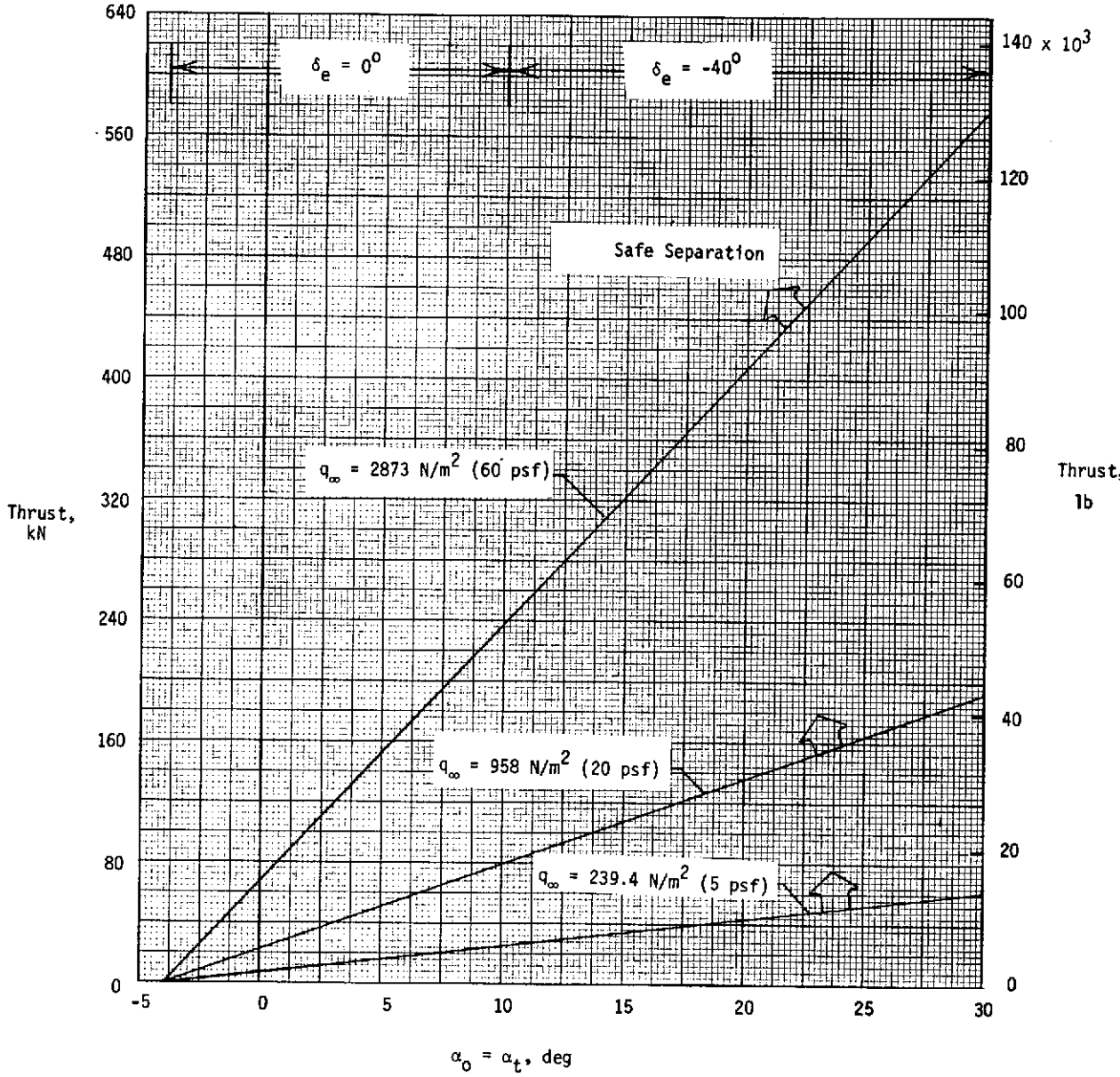

(b) $\epsilon = 38^o$.

Figure 22.- Concluded. (Note scale change.)

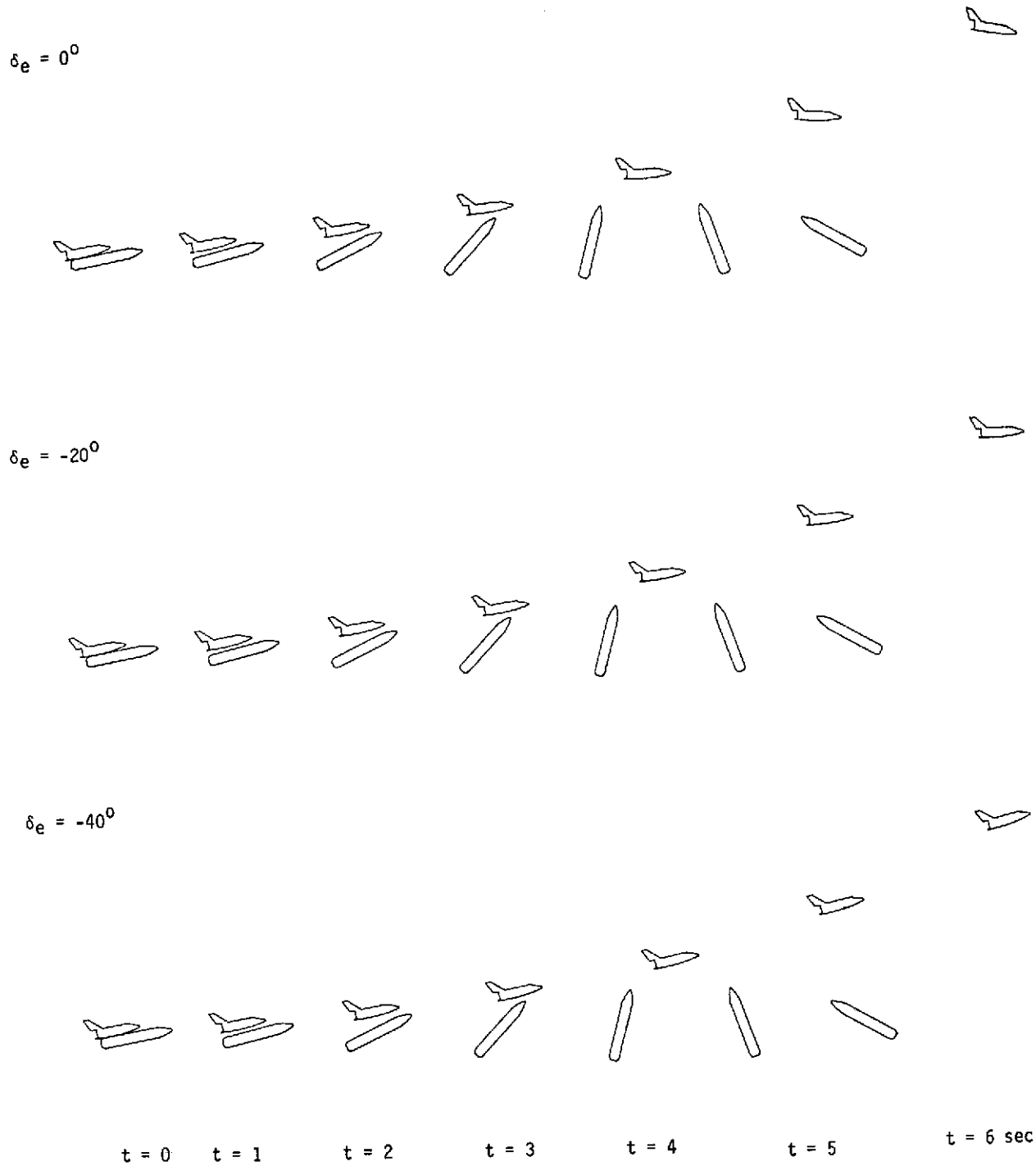

(a) Pictorial results.

Figure 23.- Effects of elevon deflection for $\alpha_o = \alpha_t = 10^o$ at t = 0. q_∞ = 2873 N/m^2 (60 psf); $\gamma = 0^o$; thrust, 222.4 kN (50 000 lb); $\epsilon = 38^o$.

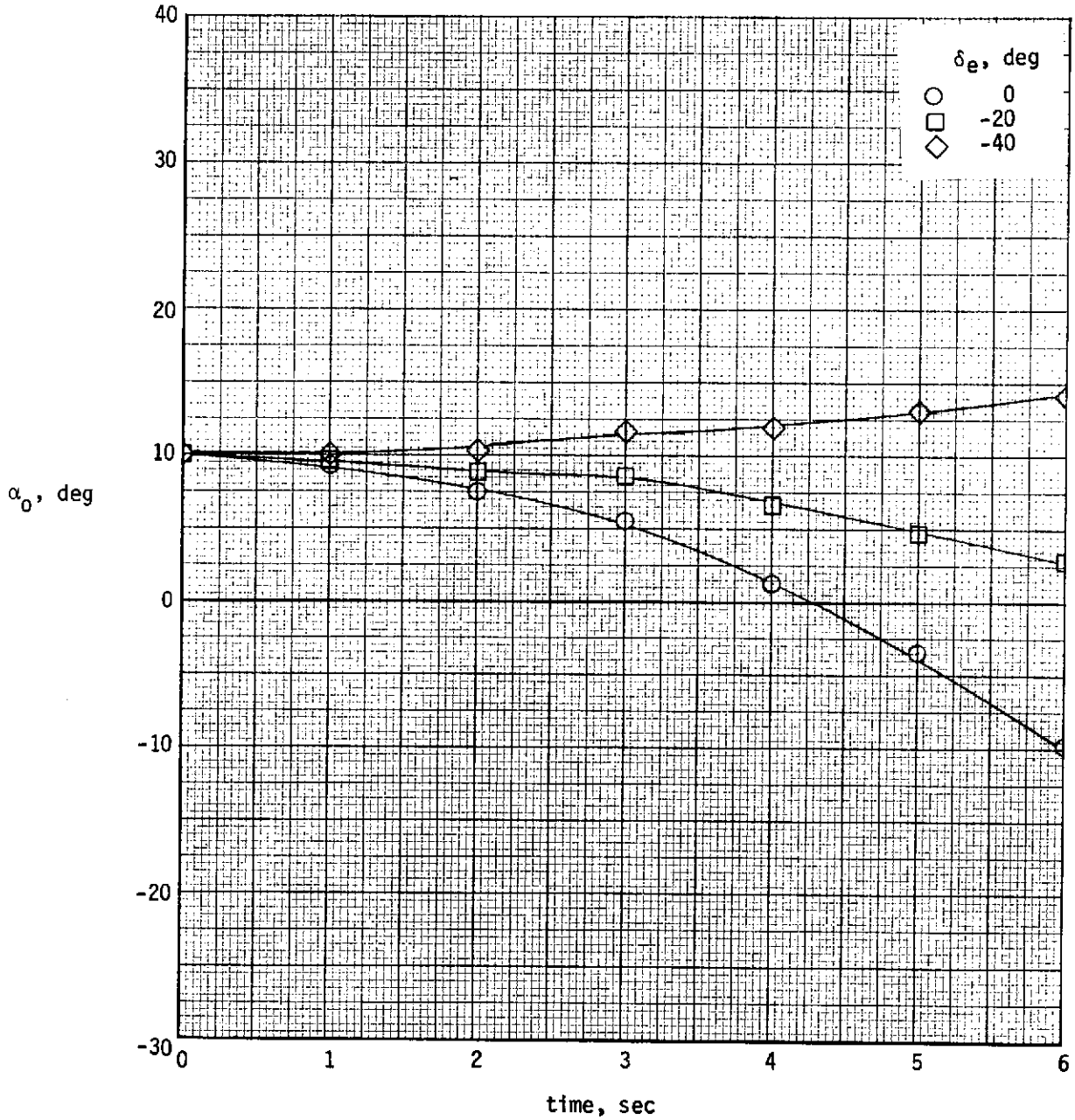

(b) Orbiter angle of attack (after release) as a function of time.

Figure 23.- Concluded.